POLITECNICO DI MILANO
Scuola di Ingegneria Civile, Ambientale e Territoriale

POLO TERRITORIALE DI COMO

Master of Science in Environmental and Geomatic Engineering

Prospectivity Modeling of Komatiite-hosted Magmatic Nickel Sulfide Mineral System in the Yilgarn Craton, Western Australia, Using ANFIS

Supervisor: Prof.Giancarlo Bernasconi

Assistant Supervisor: Dr. Alok Porwal

Master Graduation Thesis by: Devendran Aarthi Aishwarya

Student Id. Number: 765556

Academic Year 2010-2012

Acknowledgement

First of all, I thank Prof. Giorgio Guariso, Politecnico Di Milano, for granting me permission to do this work at CSRE, IITB, Mumbai, India. I can't express my gratitude and respect by merely thanking my guide, Dr. Alok Porwal, Associate Professor, CSRE. He is the one who is behind the successful completion of this project. Due to his constant motivation and guidance, I had come out with this thesis.

Since the first day of his lecture, Prof.Giancarlo Bernasconi, Associate Professor, Politecnico Di Milano, inspired me with his interesting lectures. His practical applications of the subject made me understand the concepts in depth. His teaching and ideas had framed my work into a report.

Of course, without my parents support and encouragement, I would not have been able to finish this work. I dedicate this thesis to my mom, dad and brother.

Abstract

An Adaptive NeuroFuzzy Inference System (ANFIS) is applied to model the potential of komatiite-hosted magmatic nickel sulfide mineral system in the greenstone belts of the Yilgarn Craton, Western Australia. A conceptual genetic model of the nickel-sulfide mineral system was used to identify the critical components and exploration criteria for nickel-sulfide deposits in the Yilgarn Craton at the camp scale. The exploration criteria, namely, potential nickel source rocks, potential pathways and sulfur saturation were represented in form of derivative GIS layers that were used as proxies for the exploration criteria. The derivative layers were used as model variables for developing a Takagi-Sugeno-type fuzzy inference system in the framework of nickel sulfide mineral systems.

The premise and consequent parameters of the fuzzy inference system were estimated using a hybrid learning algorithm. About 70% of the 165 known deposits of the craton were used to train the models; the remaining 30% was used to validate the models and, therefore, had to be treated as if they had not been discovered. The ANFIS predicted about 70% of the validation deposits in prospective zones that occupy about 9% of the total area occupied by the greenstone belts in the craton.

This preliminary study shows that conceptual models of mineral systems can be effectively represented by fuzzy inference systems. Moreover, by implementing a neural-network type learning algorithm, it is possible to objectively estimate the parameters of the fuzzy inference system from the spatial distribution of known mineral deposits.

Table of Contents

List of Tables

List of Figures

1. INTRODUCTION

According to Geoscience Australia's (GA) mineral fact sheet (GA, 2008), Australia contains 26.4 Million tonnes (Mt) of Economic Demonstrated Resources (EDR) of nickel, accounting for 37.5% of the world's EDR in the year 2008. It remains the largest holder of EDR of nickel followed by New Caledonia (10.1%), Russia (9.4%) and Cuba (8.0%). Russia was the largest producer of nickel in 2008 with 276 Kilotonnes (Kt) (16.9%), followed by Canada with 250 Kt (15.3%), Indonesia with 211 Kt (12.9%) and Australia with 200 Kt (12.3%). The entire production of Australian nickel comes from nickel sulfide (about 82%) and laterite (about 18%) deposits of Western Australia (Abeysinghe and Flint, 2007).

1.1 The Yilgarn Craton

The Yilgarn Craton forms the largest depository of nickel in Western Australia, containing 32,281 Kt of nickel in nickel sulfide (8431 kt) and laterite (23,850 Kt) deposits (Abeysinghe and Flint, 2007). Even though the resources are dominated by laterite nickel deposits, the bulk of production comes from magmatic nickel sulfide deposits hosted by the greenstone belts in the Yilgarn Craton. The craton contains about 20 times more nickel in the form of magmatic nickel sulfide deposits than the rest of Western Australia. It hosts more than 550 known deposits, prospects and occurrences (GSWA, 2001) including world-class deposits at Mt. Keith, Perseverance, Kambalda, Yakabindie, and Honeymoon Well. The

greenstone belts of the Eastern Superterrane contain more than 60% of the world's total nickel sulfide resources (Hoatson et al., 2006).

Western Australia, particularly Yilgarn Craton, has historically attracted considerable investments in nickel exploration, and remains one of the most intensively explored geological provinces in Australia. Nevertheless, the exploration maturity varies across the craton and there exists a significant potential for discovery of new deposits and additional resources of nickel sulfide in various parts of the craton. Based on the interpreted under-cover extensions of the known nickel sulfide-bearing greenstone sequences, Hoatson et al., (2006, p. 231) demarcated several prospective zones for magmatic nickel sulfide deposits in the north of the Perseverance-Wiluna greenstone belt, and in the Eastern Goldfields, North Eastern Goldfields, and Southern Cross provinces.

In this study, spatial mathematical-model-based integration of publicly available regional-scale geoscience datasets to delineate prospective magmatic nickel sulfide zones in the greenstone belts of the Yilgarn Craton. Adaptive Neuro Fuzzy Inference System and Weights of Evidence are used for this purpose.

2.GEOLOGY OF THE YILGARN CRATON

The Yilgarn Craton has an areal extension of about 650,000 square km with less than 5% outcropping area, thus presenting a deeply weathered profile. Based on new geological and geochronological data, Cassidy et al.(2006) reviewed the internal boundaries of the Yilgarn Craton and subdivided the craton into six terranes namely (1) Narryer Terrane in the northwest, (2) Southwest Terrane in the southwest, (3) Youanmi Terrane in centre which is an amalgamation of Murchison and Southern Cross Domains, and (4) Kalgoorlie, (5) Kurnalpi, and (6) Burtville Terranes in the eastern part of the craton. The last three terranes are bounded by interlinked fault system and jointly comprise the Eastern Goldfields Superterrane.

2.1.Six Different Terranes

The Narryer Terrane contains some of the Earth's oldest crustal segments and comprises granites and granitic gneisses interlayered with banded iron-formation, mafic and ultramafic intrusive rocks and metasedimentary rocks. The Southwest terrane is composed of granites and granitic gneisses interlayered with metasedimentary rocks, with a single preserved greenstone belt, namely, Saddleback. The Youanmi Terrane consists of greenstone rocks deposited between ca 2.9 Ga to 2.7 Ga, intruded by felsic magmatic rocks and layered mafic-ultramafic intrusions. The Eastern Goldfields Superterrane comprises dismembered

parts of greenstone sequences of slightly younger age(>2.81 Ga to ca 2.66 Ga) as compared to the Youanmi Terrane. The Ida fault forms the boundary between the Youanmi and Eastern Goldfields Terranes. The crusts in these terranes range in age from 3.8 to 3.4 Ga in the northwest for the Narryer Terrane to 2.9-2.7 Ga in the east for the Goldfields Superterrane; sedimentary sequences vary in age from 3.73 to 2.66 Ga and igneous emplacement from 3.73 to 2.63 Ga (Griffin et al., 2004; Cassidy et al., 2006).

2.1.1 Minerals in the Yilgarn Craton

Magmatic nickel sulfide mineralization is mainly hosted by the ca 2.7 Ga komatiite sequences in the greenstone belts of the Kalgoorlie Terrane. Less significant mineralization occurs in the ca. 3.03-2.72 Ga greenstone belts of the Southern Cross Domain and the ca. 2.9-2.71 Ga greenstone belts of the Kurnalpi Terrane. The Murchison Domain and Southwest Terrane are poorly mineralized (Hoarson et al., 2006). The following figures Fig.1 and Fig.2 show the boundary and the Geology maps of the study area.

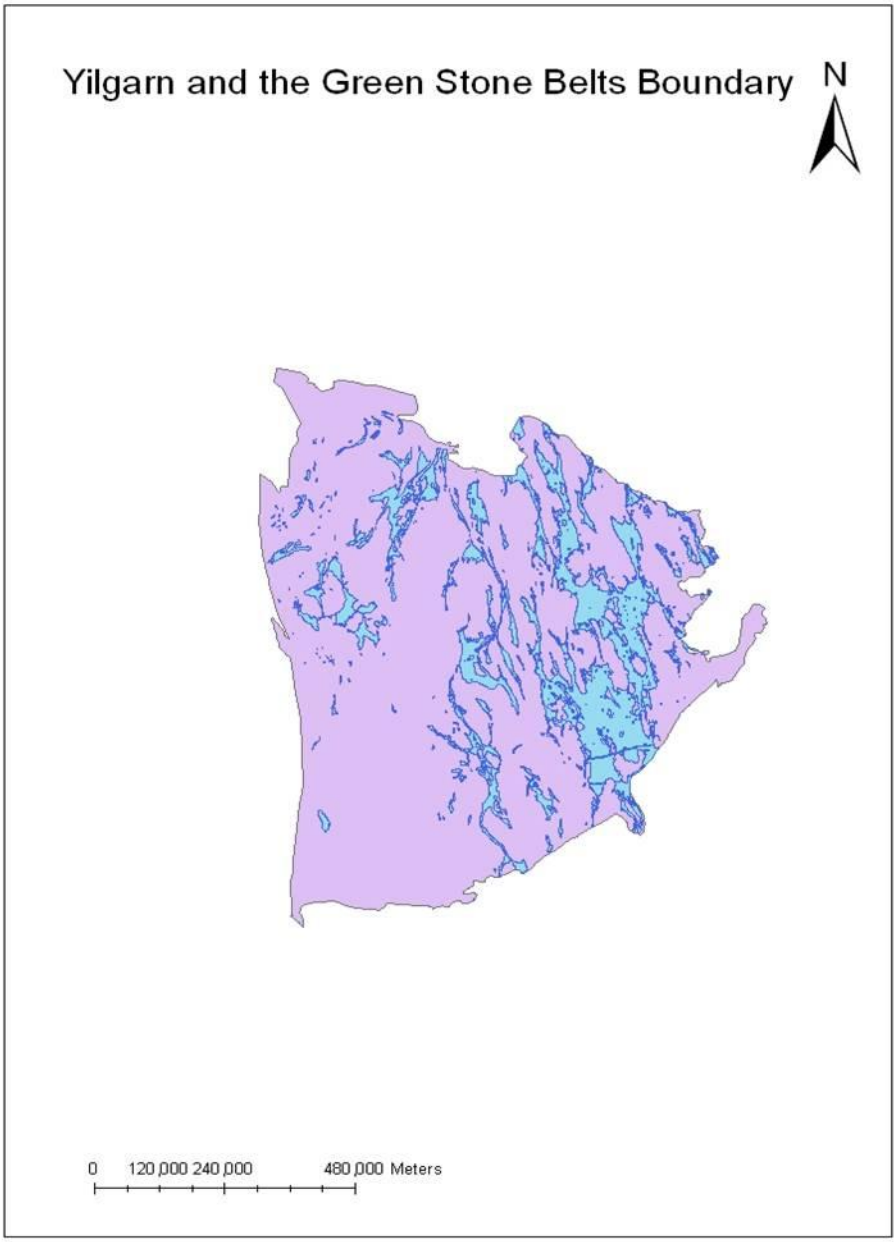

Fig.1 Yilgarn and Greenstones Boundaries

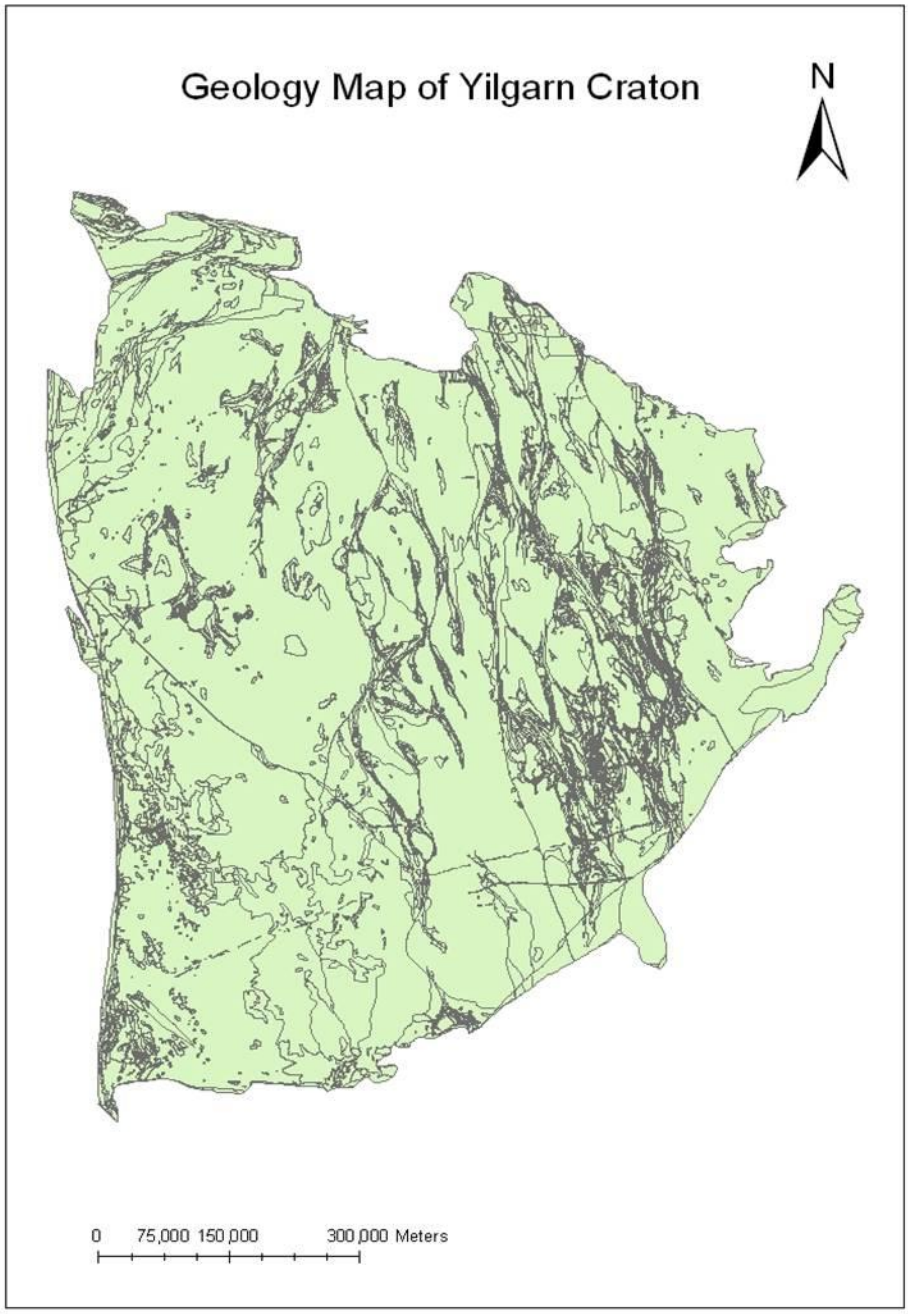

Fig.2 Geology of the study area

The geological details of the study area are represented as attribute table and are shown in the following figure 3.

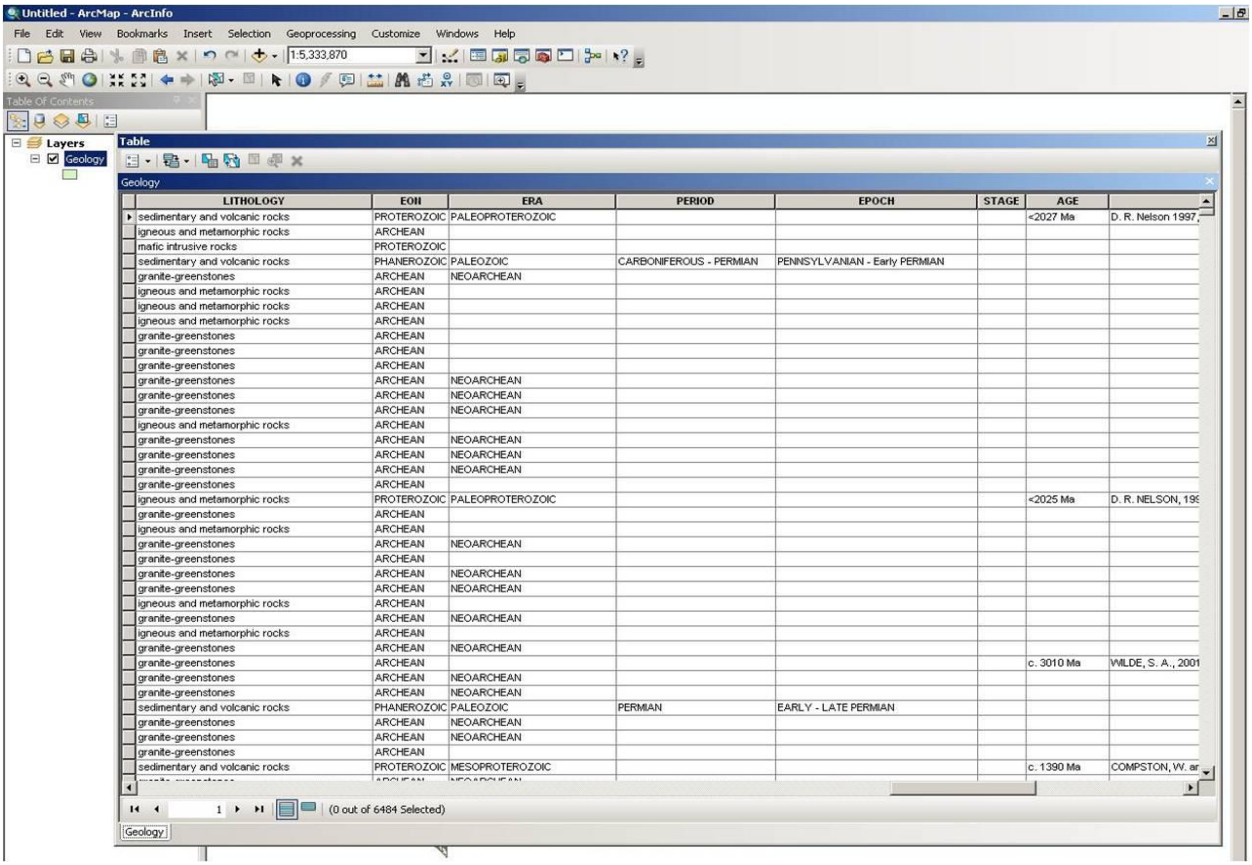

LITHOLOGY	EON	ERA	PERIOD	EPOCH	STAGE	AGE	
sedimentary and volcanic rocks	PROTEROZOIC	PALEOPROTEROZOIC				<2027 Ma	D. R. Nelson 1997,
igneous and metamorphic rocks	ARCHEAN						
mafic intrusive rocks	PROTEROZOIC						
sedimentary and volcanic rocks	PHANEROZOIC	PALEOZOIC	CARBONIFEROUS - PERMIAN	PENNSYLVANIAN - Early PERMIAN			
granite-greenstones	ARCHEAN	NEOARCHEAN					
igneous and metamorphic rocks	ARCHEAN						
igneous and metamorphic rocks	ARCHEAN						
igneous and metamorphic rocks	ARCHEAN						
granite-greenstones	ARCHEAN						
granite-greenstones	ARCHEAN						
granite-greenstones	ARCHEAN						
granite-greenstones	ARCHEAN	NEOARCHEAN					
granite-greenstones	ARCHEAN	NEOARCHEAN					
granite-greenstones	ARCHEAN	NEOARCHEAN					
igneous and metamorphic rocks	ARCHEAN						
granite-greenstones	ARCHEAN	NEOARCHEAN					
granite-greenstones	ARCHEAN	NEOARCHEAN					
granite-greenstones	ARCHEAN	NEOARCHEAN					
granite-greenstones	ARCHEAN						
igneous and metamorphic rocks	PROTEROZOIC	PALEOPROTEROZOIC				<2025 Ma	D. R. NELSON, 19
granite-greenstones	ARCHEAN						
igneous and metamorphic rocks	ARCHEAN						
granite-greenstones	ARCHEAN	NEOARCHEAN					
granite-greenstones	ARCHEAN						
granite-greenstones	ARCHEAN	NEOARCHEAN					
granite-greenstones	ARCHEAN	NEOARCHEAN					
igneous and metamorphic rocks	ARCHEAN						
granite-greenstones	ARCHEAN	NEOARCHEAN					
igneous and metamorphic rocks	ARCHEAN						
granite-greenstones	ARCHEAN	NEOARCHEAN					
granite-greenstones	ARCHEAN					c. 3010 Ma	WILDE, S. A., 2001
granite-greenstones	ARCHEAN	NEOARCHEAN					
granite-greenstones	ARCHEAN	NEOARCHEAN					
sedimentary and volcanic rocks	PHANEROZOIC	PALEOZOIC	PERMIAN	EARLY - LATE PERMIAN			
granite-greenstones	ARCHEAN	NEOARCHEAN					
granite-greenstones	ARCHEAN	NEOARCHEAN					
granite-greenstones	ARCHEAN						
sedimentary and volcanic rocks	PROTEROZOIC	MESOPROTEROZOIC				c. 1390 Ma	COMPSTON, W. ar

Fig 3. Attribute table of the Geology of the study area

3.ADAPTIVE NEURO FUZZY SYSTEMS: THEORETICAL BACKGROUND

3.1. Comparison between Manual Tuning Process and Fuzzy System

One benefit of fuzzy systems (Zadeh, 1965; Ruspini et al., 1998; Cox, 1994) is that the rule base can be created from expert knowledge, used to specify fuzzy sets to partition all variables and a sufficient number of fuzzy rules to describe the input/output relation of the problem at hand. However, a fuzzy system that is constructed by expert knowledge alone will usually not perform as required when it is applied because the expert can be wrong about the location of the fuzzy sets and the number of rules. A manual tuning process must usually be appended to the design stage which results in modifying the membership functions and/or the rule base of the fuzzy system. This tuning process can be very time consuming and error-prone. Also, in many applications expert knowledge is only partially available or not at all. It is therefore useful to support the definition of the fuzzy rule base by automatic learning approaches that make use of available data samples. This is possible since, once the components of the fuzzy system is put in a parametric form, the fuzzy inference system becomes a parametric model which can be tuned by a learning procedure. Fuzzy logic and artificial neural networks (Haykin, 1998; Mehrotra et al., 1997) are complementary

technologies in the design of intelligent systems. The combination of these two technologies into an integrated system appears to be a promising path toward the development of Intelligent Systems capable of capturing qualities characterizing the human brain. Both neural networks and fuzzy logic are powerful design techniques that have their strengths and weaknesses. The integrated system will have the advantages of both neural networks (e.g. learning abilities, optimization abilities and connectionist structures) and fuzzy systems (human like IF-THEN rules thinking and ease of incorporating expert knowledge) (Brown & Harris,1994). In this way, it is possible to bring the low-level learning and computational power of neural networks into fuzzy systems and also high-level human like IF-THEN thinking and reasoning of fuzzy systems into neural networks. Thus, on the neural side, more and more transparency is pursued and obtained either by pre-structuring a neural network to improve its performance or by possible interpretation of the weight matrix following the learning stage. On the fuzzy side, the development of methods allowing automatic tuning of the parameters that characterize the fuzzy system can largely draw inspiration from similar methods used in the connectionist community. This combination does not usually mean that a neural network and a fuzzy system are used together in some way.

3.2 Neuro-Fuzzy Method

The neuro-fuzzy method is rather a way to create a fuzzy model from data by some kind of learning method that is motivated by learning procedures used in neural networks. This substantially reduces development time and cost while improving the accuracy of the resulting fuzzy model. Being able to utilize a neural learning algorithm implies that a fuzzy system with linguistic information in its rule base can be updated or adapted using numerical information to gain an even greater advantage over a neural network that cannot make use of linguistic information and behaves as a black-box. Equivalent terms for neurofuzzy systems that can be found in the literature are neural fuzzy or sometimes neuro-fuzzy networks (Buckley and Eslami, 1996). Neuro-fuzzy systems are basically adaptive fuzzy systems developed by exploiting the similarities between fuzzy systems and certain forms of neural networks, which fall in the class of generalized local methods. Hence, the behavior of a neuro-fuzzy system can either be represented by a set of humanly understandable rules or by a combination of localized basis functions associated with local models (i.e. a generalized local method), making them an ideal framework to perform nonlinear predictive modeling. Nevertheless, one important consequence of this hybridization between the representational aspect of fuzzy models and the

learning mechanism of neural networks is the contrast between readability and performance of the resulting model.

3.2.1 Advantages of implementing ANFIS

Summarizing, neural networks can improve their transparency, making them closer to fuzzy systems, while fuzzy systems can self-adapt, making them closer to neural networks (Lin & Lee, 1996). Fuzzy systems can be seen as a special case of local modeling methods, where the input space is partitioned into a number of fuzzy regions represented by multivariate membership functions. For each region, a rule is defined that specifies the output of the system in that region. The class of functions that can be accurately reproduced by the resulting model is determined by the nonlinear mapping performed by the multivariate fuzzy membership functions. This impressive result allows comparison to be drawn between fuzzy systems and the more conventional techniques referred to as generalized local methods. In particular, if bell-shaped (Gaussian) membership functions are used, then a Takagi-Sugeno (TS) fuzzy system is equivalent to a special kind of Radial Basis Function (RBF) network (Jang & Sun, 1993). Theorems and analysis derived for local modeling methods can directly be applied to fuzzy systems. Also, due to this similarity, fuzzy

systems allow relatively easy application of learning techniques used in local methods for identification of fuzzy rules from data. On the other side, fuzzy systems distinguish from other local modeling techniques, for their potentiality of an easy pre-structuring and a convenient integration of a priori knowledge. Many learning algorithms from the area of local modeling, and more specifically techniques developed for some kind of neural networks, have been extended to automatically extract or tune fuzzy rules based on available data. All these techniques exploit the fact that, at the computational level, a fuzzy system can be seen as a layered architecture, similar to an artificial neural network. By doing so, the fuzzy system becomes a neuro-fuzzy system, i.e. special neural network architecture. In 1991, Lin and Lee have proposed the very first implementation of Mamdani fuzzy models using layered feed-forward architecture (Lin & Lee, 1991). Nevertheless, the most famous example of neuro-fuzzy network is the Adaptive Network-based Fuzzy Inference System (ANFIS) developed by Jang in 1993 (Jang, 1993), that implements a TS fuzzy system in a network architecture, and applies a mixture of plain back-propagation and least mean squares procedure to train the system.

3.3 Architecture of ANFIS

Adaptive Neuro-Fuzzy Inference System (ANFIS) is one of the most successful schemes which combine the benefits of these two powerful paradigms into a single capsule (Jang, 1993). An ANFIS works by applying neural learning rules to identify and tune the parameters and structure of a Fuzzy Inference System (FIS). There are several features of the ANFIS which enable it to achieve great success in a wide range of scientific applications. The attractive features of an ANFIS include: easy to implement, fast and accurate learning, strong generalization abilities, excellent explanation facilities through fuzzy rules, and easy to incorporate both linguistic and numeric knowledge for problem solving (Jang & Sun, 1995; Jang et al., 1997). According to the neuro-fuzzy approach, a neural network is proposed to implement the fuzzy system, so that structure and parameter identification of the fuzzy rule base are accomplished by defining, adapting and optimizing the topology and the parameters of the corresponding neuro-fuzzy network, based only on the available data. The network can be regarded both as an adaptive fuzzy inference system with the capability of learning fuzzy rules from data, and as a connectionist architecture provided with linguistic meaning. A typical architecture of an

ANFIS, in which a circle indicates a fixed node, whereas a square indicates an adaptive node, is shown in Figure 4.

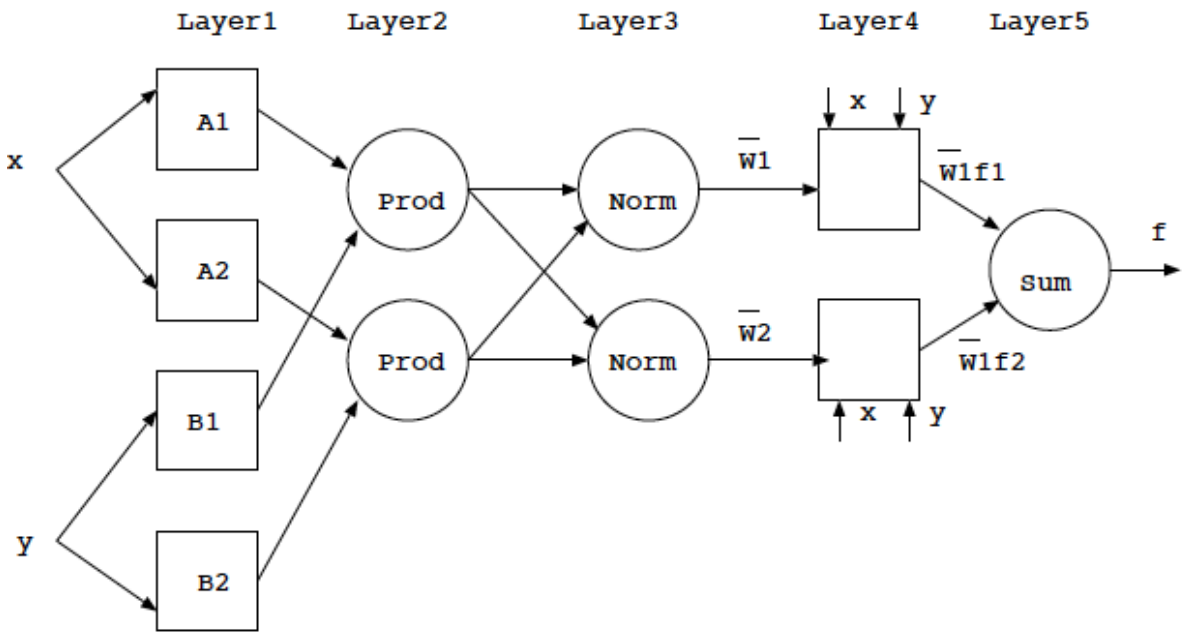

Fig 4. Typical architecture of an ANFIS model

In this connectionist structure, there are input and output nodes, and in the hidden layers, there are nodes functioning as membership functions (MFs) and rules. This eliminates the disadvantage of a normal feed forward multilayer network, which is difficult for an observer to understand or to modify. For simplicity, we assume that the examined FIS has two inputs and one output. For a first-order Sugeno fuzzy model, a typical rule set with two fuzzy "ifthen" rules can be expressed as follows:

Rule 1: If x is A1 and y is B1, then f1 = p1 x + q1 y + r1

Rule 2: If x is A2 and y is B2, then f2 = p1 x + q2 y + r2

Where x and y are the two crisp inputs, and Ai and Bi are the linguistic labels associated with the node function. As indicated in above figure, the system has a total of five layers.

ANFIS are a class of adaptive networks that are functionally equivalent to fuzzy inference systems. ANFIS represent Sugeno and Tsukamoto fuzzy models. ANFIS uses a hybrid learning algorithm. Assume that the fuzzy inference system has two inputs x and y and one output z.

A first-order Sugeno fuzzy model has rules as the following:

• Rule 1: If x is A1 and y is B1, then f1 = p1x + q1y + r1

• Rule 2: If x is A2 and y is B2, then f2 = p2x + q2y + r2

Layer 1 - I

Ol,i is the output of the ith node of the layer l.

• Every node i in this layer is an adaptive node with a node function

$O_{1,i} = \mu A_i(x)$ for i = 1, 2, or

$O_{1,i} = \mu B_{i-2}(x)$ for i = 3, 4

• X (or y) is the input node i and Ai (or Bi−2) is a linguistic label associated with this node

• Therefore O1, i is the membership grade of a fuzzy set (A1, A2, B1, B2).

Layer 1- II

Typical membership function:

$$\mu_A(x) = \frac{1}{1 + \left|\frac{x-c_i}{a_i}\right|^{2b_i}}$$

- ai, bi, ci is the parameter set.
- Parameters are referred to as premise parameters

Layer 2

• Every node in this layer is a fixed node labeled Prod.

• The output is the product of all the incoming signals.

• O2,i = wi = μAi(x) · μBi(y), i = 1, 2

• Each node represents the fire strength of the rule

• Any other T-norm operator that perform the AND operator can be used

Layer 3

• Every node in this layer is a fixed node labeled norm.

• The ith node calculates the ratio of the ith rule's firing strength to the sum of all rules firing strengths.

$$O_{3,i} = \overline{w}_i = \frac{w_i}{w_1 + w_2}, \quad i = 1, 2$$

• Outputs are called normalized firing strengths.

Layer 4

• Every node i in this layer is an adaptive node with a node function:

$$O_{4,1} = \overline{w}_i f_i = \overline{w}_i (p_x + q_i y + r_i)$$

• w_i is the normalized firing strength from layer 3.

• $\{p_i, q_i, r_i\}$ is the parameter set of this node.

• These are referred to as consequent parameters

Layer 5

• The single node in this layer is a fixed node labeled sum, which computes the overall output as the summation of all incoming signals:

$$overall\ output = O_{5,1} = \sum_i \overline{w}_i f_i = \frac{\sum_i w_i f_i}{\sum_i w_i}$$

3.3.1 Hybrid Learning Algorithm

• The ANFIS can be trained by a hybrid learning algorithm

• In the forward pass the algorithm uses least-squares method to identify the consequent parameters on the layer 4.

• In the backward pass the errors are propagated backward and the premise parameters are updated by gradient descent.

4.BAYESIAN PROBABILISTIC MODELS: THEORETICAL BACKGROUND OF THE WEIGHTS OF EVIDENCE MODEL

4.1 Weights of Evidence

A variety of new tools are available for use in GIS for evaluating the distribution of phenomena in a statistical framework. A weight of Evidence is one such tool which was initially applied in GIS to predict the occurrence of minerals based on known mineral deposits. Weights are estimated for a set of evidential themes associated with the known occurrences. These weights are then evaluated for the evidential themes in an area to produce a map of potential values for occurrence of that mineral. A weight of evidence model is used to predict occurrence of an event with known evidences in a study area where training data are available to estimate the relative importance of each evidence by statistical methods. It provides a quantitative method for integrating multiple sources of evidences. It avoids subjective choice of evidences and subjective estimation of weights for evidences with comparing with other methods, such as Fuzzy logic method.

4.2 GIS and Weights of Evidence

A Geographical Information System (GIS) is a "computer-based system which integrates the data input, data storage and management, data

manipulation and analysis and data output for both spatial and attribute data to support decision-making activities" (Malczewski, 1999). After over 40 years of development, GIS have been applied to serve important roles in many fields, such as environment monitoring, resources management, applications in commerce and business field, and different utilities. The ultimate purpose of GIS is to make evaluations or predictions with different specific data integration models to combine spatial and attribute data from various sources to provide support for decision-makers.

According to Bonham-Carter (1994), the data integration models in GIS are divided into two categories, data-driven and knowledge-driven models based on different methods for estimation of weights of different evidential maps. In data-driven models, the weights are calculated by using statistical methods and data of evidences in a training area to estimate the spatial relationships between the evidential maps and the final response maps. Data-driven models include Logistic Regression, Weights of Evidence, Neural Network, and so on, and the weights in those models are calculated from training data. While, the weights are estimated based on experts' opinions in knowledge-driven models. The knowledge-driven models

include Fuzzy Logic, Dempster-Shafer Belief Theory and their weights are given with experts' opinions.

4.3 Weights of Evidence in Mineral mapping

Weights of evidence model is used to predict a hypothesis about occurrence of an event based on combining known evidence in a study area where sufficient data are available to estimate the relative importance of each evidence by statistical methods. In the case of mineral resources assessment, the evidence consists of a set of evidential dataset (maps) and the model is used to predict the hypothesis about the occurrence of a given type of deposit in a study area. The weights are estimated from the measured association between known mineral occurrences and the values on the evidential maps. Based on combination of the evidential maps selected, the final result is extracted as a mineral potential map with a single index representing probability of occurrence of the given type of mineral deposit.

4.3.1 Model Development

The model was originally developed for prediction of the probability that a new patient would be diagnosed to have a disease based on presence or absence of set symptoms (Kemp et

al. 1999). Currently, it is still used in the medical fields (Zuyle. 2000; Johnson et al., 2001). The model has been applied in mineral resources assessment or geological survey with GIS together since the late 1980s (Agterberg, 1989, Agterberg, et al. 1993; Bonham-carter, 1991; Bonham-carter, et al. 1989). For example, this method was applied to predict occurrence of gold deposits in Nova Scotia (Bonham.carter, et al. 1988; Cheng et al:, 1999) and other places (Harris et al., 2000; Raines, 1999). This model is also used in evaluation on distribution of other resources such as copper deposits (Tangestani et al., 2001), fossil packrat (Neotoma) middens (Mensing et al., 2000) and archaeology sites in a portion of the Central Valley of California (Hansen, 2000). Currently, weights of evidence model have been implemented in ArcView GIS (Arc-WofE) (Kemp et al., 1999 and 2001). Arc-WofE has been widely used in mineral exploration and environmental assessments (Hansen, 2000; Zuyle, 2000).

4.4 Probability behind Weights of Evidence

Weights of evidence model uses a probability framework based on set theory (Bonham.Carter, 1994). One of the important concepts used in this

approach is the idea of prior and posterior probability. In the situation of mineral resource assessment, assume that a hypothesis (H) about the probability of mineral deposits of a given type D of in a study area is related to a set of evidence X (X = (X1, X2,....,Xn), and X1, X2,...., Xn are conditionally independent with each other).

The prior probability (P {A}) is the probability of occurrence of mineral deposit of type A without consideration of any known evidence information. The posterior probability (P {A} |X), also named conditional probability, is the probability of occurrence of mineral deposit of type A given the condition of X existing in the study area.

4.4.1 Odd probability Concept

Another concept used here is odd (O{A}), which is defined as a ratio of the probability that an event will occur, such as P(A), to the probability that it will not occur, such as P($\bar{A}$)It can be expressed as following equation:

$$O(A) = P(A) / P(\bar{A})$$

As to the hypothesis H on A with given X, its odd is:

$$O(A|X) = O(A).P(A|X) / P(\bar{A}|X)$$

In ordinary weights of evidence model, each evidence Xi in X need be divided into two subsets which can be expressed in terms of

set theory: A (presence or true) and $\bar{A}$ (absence or false). The two subsets have following properties:

1) A U A = Xi (A and A make up Xi), i = 1, 2… n

2) $A \cap A = 0$ (A and A are mutually exclusive)

According to definitions and the properties of binary patterns, the following equations can be derived:

$$P(A|X) = P(A).\ P(X|A) / P(X)$$

$$= P(A).\ P(X1|A).P(X2|A).....P(Xn|D) / P(X1).P(X2)....P(Xn)$$

$$O(A|X) = O(A).\ P(X|A) / P(X|A)$$

$$= O(A).\ P(X1|A).P(X2|A)....P(Xn|A) / P(X1|A).P(X2|A)....P(Xn|A)$$

$$Log(O(A|X)) = Log(O(A)) + Log\ P(X|A)/ P(X|A)$$

$$= Log(O(A)) + Log\ (P(X1|A)) / P(X1|A) + Log\ (P(X2|A) / P(X2|A)) +.....+ Log\ (P\ (Xn|A) / P\ (Xn|A)\ )$$

If Xi is present, P (Xi|A) / P (Xi|A) is called sufficient ratio (LS). Otherwise, it is called necessity ratio (LN). Correspondingly, the natural logarithm of LS is the positive weight (W+) and the natural logarithm of LN is the negative weight of evidence (W-). For convenience, let W0 denote the natural logarithm of O (A).

Thus, O (A|X) = O (A) LS1 (or LN1) LS2 (or LN2)....LSn(or LNn)

Log (O (A|X)) = W0+W1 + (or W1-) + W2+ (or W2-) +....+ Wn +(or Wn-) = sum Wi

Then, the posterior probability P (A|X) can be converted from the equation above as follows:

P(A|X) = exp(Logit(O(A|X))) / 1+exp(Logit(O(A|X)))

The values of P(A|X) calculated with using the above equation are identical to those calculated directly using the previous equations. The advantage of using weights, instead of directly using the conditional probability expressions is that the weights are easier to be interpreted than the probability factors.

In most applications of ordinary weights of evidence model, the contrast C is used to select the cutoff to divide continuous variables into binary patterns.

$$C = Wi+ - Wi-, i = 1,2,...,n$$

5. CONCEPTUAL MODEL OF MAGMATIC NICKEL - SULFIDE MINERAL SYSTEM

5.1. Nickel Sulfide ore formation

Nickel-copper sulfide deposits are found at the base of mafic and ultramafic bodies. All their host rocks, except the Sudbury Igneous Complex, are thought to be mantle-derived melts. The Sudbury Igneous Complex is thought to be the product of complete melting of continental crust. In the case of mantle-derived magmas, a high degree of partial melting of the mantle serves to enrich the silicate magma in Ni and platinum group elements (PGE). This magma is then transported to the crust by an efficient process in order to reduce the possibility that Ni is removed from the magma by crystallization of olivine. Once the magma is emplaced into the crust, sulphur from some source gets added to bring about saturation of the base metal sulfide liquid. An ideal site for all of these processes is where a mantle plume intersects a continental rift. The plume provides a large volume of magma, produced by a high degree of partial melting. The normal faults of the rift provide easy access to the crust so that the magma is transported efficiently. In many cases rifts contain sedimentary rocks rich in sulphur, thus providing an ideal source of sulphur for sulfide saturation. The heat

from the plume can lead to melting of a large volume of rift sediments and release of sulphur from the sediments to the Ni-PGE•rich primary magma. In the case of the Sudbury Igneous Complex, a very large volume of superheated magma formed by flash melting of the crust. This melting event is the result of the impact of shock waves from the explosion of a large meteor in the atmosphere.

5.1.1 Geological Process of formation of the ore

In both the case of mantle-derived magma and the case of the Sudbury Igneous Complex, once sulfide liquid formed as suspended droplets in the silicate magma it must have interacted with a large volume of mafic magma in order to become enriched in Ni, Cu, and PGE in the sulfide. This enrichment occurred when the droplets were transported or when they were suspended in eddies. The magma from which the Sudbury Igneous Complex formed was superheated and base metal sulfide liquid formed at approximately 200°C above the magma liquidus. Thus the Sudbury sulfide liquid had more time to equilibrate with the silicate magma than a sulfide droplet in a mantle-derived magma. This extra time and the huge volume of silicate magma in the melt sheet allowed the sulfide liquid to maximize the concentration of Ni, Cu, and PGE. The efficiency of the metal

collection step in the case of the Sudbury Igneous Complex counterbalanced the fact that this crustal derived magma had lower Ni and PGE contents than most mantle-derived magmas. The sulfide droplets collected at the base of intrusions and lava flows because they are denser than the silicate magma. The largest concentrations are typically found in locations where there are changes in the geometry of the contacts between intrusions or flows and the country rock. In some cases the accumulated sulfide liquid fractionated to form an Fe-rich monosulfide solid-solution (mss) cumulate and a Cu-rich sulfide liquid which later crystallized as an intermediate solid solution (iss). As a result of crystal fractionation of mss many Ni sulfide orebodies show a strong zonation with respect to Cu and PGE. During mss fractionation Os, Ir, Ru, and Rh concentrated in the mss cumulate and Cu, Pt, Pd, and Au concentrated in the Cu-rich sulfide liquid. The partition coefficient for Ni into mss is close to 1; thus, mss fractionation would not have caused large variations in Ni concentrations. The silicate magma solidified at or above 1,000°C whereas the Cu-rich sulfide liquid solidified at ~900°C. Thus, at many localities the Cu-rich sulfide liquid appears to have migrated into dilatent spaces in the footwall or the hanging wall to form veins that

extend into the country rock for up to 2 km. At subsolidus temperatures a number of processes modify the orebodies. Both the mss and iss are not stable below 600°C. As the sulfides cooled mss exsolved to form pyrrhotite and pentlandite (±pyrite), and iss exsolved to form chalcopyrite and pyrrhotite (±cubanite, ±pyrite). Most of the PGE and chalcophile elements that originally partitioned into mss or iss are not readily accommodated in the structure of pyrrhotite, pentlandite, and chalcopyrite; therefore, they exsolve from the mss and iss at low temperature and form a wide variety of platinum group minerals (PGM). During deformation stress may focus in the structurally incompetent massive sulfide units, which are generally located at the lower contact of the mafic or ultramafic host rock. In this situation the massive sulfides may then be displaced relative to the host rocks. Finally, during greenschist to amphibolite metamorphism, olivine is unstable and Ni released from the olivine will partition into disseminated sulfides, thereby upgrading the sulfides.

5.2 Theories of Ore genesis

The various theories of ore genesis explain how the various types of mineral deposits form within the Earth's crust. Ore genesis

theories are very dependent on the mineral or commodity. Ore genesis theories generally involve three components: source, transport or conduit, and trap. This also applies to the petroleum industry, which was first to use this methodology.

- Source is required because metal must come from somewhere, and be liberated by some process
- Transport is required first to move the metal bearing fluids or solid minerals into the right position, and refers to the act of physically moving the metal, as well as chemical or physical phenomenon which encourage movement
- Trapping is required to concentrate the metal via some physical, chemical or geological mechanism into a concentration which forms mineable ore

The biggest deposits are formed when the source is large, the transport mechanism is efficient, and the trap is active and ready at the right time.

5.2.1 Ore genesis processes

Evans (1993) divides ore genesis into the following main categories based on physical process. These are internal processes, hydrothermal processes, metamorphic processes and surficial processes.

5.2.2 Internal processes

These processes are integral physical phenomena and chemical reactions internal to magmas, generally in plutonic or volcanic rocks. These include;

- Fractional crystallization, either creating monomineralic cumulate ores or contributing to the enrichment of ore minerals and metals
- Liquidation, or liquid immiscibility between melts of differing composition, usually sulfide segregations of nickel-copper-platinoid sulfides and silicates.

5.2.3 Hydrothermal processes

These processes are the physico-chemical phenomena and reactions caused by movement of hydrothermal waters within the crust, often as a consequence of magmatic intrusion or tectonic upheavals. The foundations of hydrothermal processes are the source-transport-trap mechanism. Sources of hydrothermal solutions include seawater and meteoric water circulating through fractured rock, formational brines (water trapped within sediments at deposition) and metamorphic fluids created by dehydration of hydrous minerals

during metamorphism. Metal sources may include a plethora of rocks. However most metals of economic importance are carried as trace elements within rock-forming minerals, and so may be liberated by hydrothermal processes. This happens because of:

- incompatibility of the metal with its host mineral, for example zinc in calcite, which favours aqueous fluids in contact with the host mineral during diagenesis.
- solubility of the host mineral within nascent hydrothermal solutions in the source rocks, for example mineral salts (halite), carbonates (cerussite), phosphates (monazite and thorianite) and sulfates (barite)
- elevated temperatures causing decomposition reactions of minerals

Transport by hydrothermal solutions usually requires a salt or other soluble species which can form a metal-bearing complex. These metal-bearing complexes facilitate transport of metals within aqueous solutions, generally as hydroxides, but also by processes similar to chelation.

This process is especially well understood in gold metallogeny where various thiosulfate, chloride and other gold-carrying chemical

complexes (notably tellurium-chloride/sulfate or antimony-chloride/sulfate). The majority of metal deposits formed by hydrothermal processes include sulfide minerals, indicating sulfur is an important metal-carrying complex.

5.2.4 Sulfide deposition

Sulfide deposition within the trap zone occurs when metal-carrying sulfate, sulfide or other complexes become chemically unstable due to one or more of the following processes;

- falling temperature, which renders the complex unstable or metal insoluble
- loss of pressure, which has the same effect
- reaction with chemically reactive wall rocks, usually of reduced oxidation state, such as iron bearing rocks, mafic or ultramafic rocks or carbonate rocks
- degassing of the hydrothermal fluid into a gas and water system, or

boiling, which alters the metal carrying capacity of the solution and even destroys metal-carrying chemical complexes

Metal can also become precipitated when temperature and pressure or oxidation state favour different ionic complexes in the water, for instance the change from sulfide to sulfate, oxygen fugacity, exchange of metals between sulfide and chloride complexes, et cetera.

5.2.5.Metamorphic processes

Lateral secretion

Ore deposits formed by lateral secretion are formed by metamorphic reactions during shearing, which liberate mineral constituents such as quartz, sulfides, gold, carbonates and oxides from deforming rocks and focus these constituents into zones of reduced pressure or dilation such as faults. This may occur without much hydrothermal fluid flow, and this is typical of podiform chromite deposits. Metamorphic processes also control many physical processes which form the source of hydrothermal fluids, outlined above.

5.2.6 Surficial processes

Surficial processes are the physical and chemical phenomena which cause concentration of ore material within the regolith, generally by the action of the environment. This includes placer deposits, laterite deposits and residual or eluvial deposits. The physical processes of ore deposit formation in the surficial realm include;

- erosion
- deposition by sedimentary processes, including winnowing, density separation (e.g.; gold placers)
- weathering via oxidation or chemical attack of a rock, either liberating rock fragments or creating chemically deposited clays, laterites or manto ore deposits
- Deposition in low-energy environments in beach environments

5.3 Occurrence of Nickel

Nickel deposits are generally found in two forms, either as sulfide or laterite. Sulfide type nickel deposits are formed in essentially the same manner as platinum deposits. Nickel is a chalcophile element which prefers sulfides, so an ultramafic

or mafic rock which has a sulfide phase in the magma may form nickel sulfides. The best nickel deposits are formed where sulfide accumulates in the base of lava tubes or volcanic flows — especially komatiite lavas. Komatiitic nickel-copper sulfide deposits are considered to be formed by a mixture of sulfide segregation, immiscibility, and thermal erosion of sulfidic sediments. The sediments are considered to be necessary to promote sulfur saturation. Some subvolcanic sills in the Thompson Belt of Canada host nickel sulfide deposits formed by deposition of sulfides near the feeder vent. Sulfide was accumulated near the vent due to the loss of magma velocity at the vent interface. The massive Voisey's Bay nickel deposit is considered to have formed via a similar process. The process of forming nickel laterite deposits is essentially similar to the formation of gold laterite deposits, except that ultramafic or mafic rocks are required. Generally nickel laterites require very large olivine-bearing ultramafic intrusions. Minerals formed in laterite nickel deposits include gibbsite.

6. MINERALIZATION PROCESSES TO PREDICTOR MAPS: DATA PREPROCESSING

6.1 Process of mineralization

Magmatic nickel sulfide deposits form in dynamic lava channels or magma conduits from sulfur-undersaturated mafic-ultramafic magmas by magmatic processes (crystallization, differentiation and concentration) and assimilation of crustal sulfur (Keays 1995: Lesher et al., 2001).

The mineralization processes for the formation of magmatic nickel sulfide deposits are:

- Formation of nickel-rich, primitive, sulfur-undersaturated, mafic-ultramafic source magma
- Emplacement of the source magma in upper-crustal levels
- Saturation of the source magma with respect to sulfur and segregation of immiscible nickel sulfide liquid.

The above mentioned processes can be translated into the following exploration criteria for nickel sulfide deposits. Thus, the exploration criteria

(1) Presence of potential nickel source rocks, (2) favourable geological settings and pathways, and (3) sulfur saturation, were represented as predictor maps.

6.2 Presence Of Potential Nickel Source Rocks

In the Yilgarn Craton, Archaean komatiite flows are considered as the most important source rocks for nickel sulfide deposits. Any high MgO ultramafic rock could be a potential source of nickel because of high nickel abundance in the olivine fraction. The higher the MgO content of an ultramafic suite and the more primitive it is, the higher the olivine abundance and, therefore the nickel content.

Hoatson et al. (2006) suggest that fertile komatiitic provinces are dominated by aluminium-undepleted komatiites (AUDK), although aluminium-depleted komatiites (ADK) also host significant komatiite deposits.

Hence, the following predictor maps were prepared from the Geological Survey of Western Australia's interpreted bed rock geological map and geochemistry dataset:

- Komatiite/mafic-ultramafic rocks
- High MgO content
- Al2O3/TiO2 ratio

The Geochemistry and the structures map of the region are shown in the figures 5 and 6.

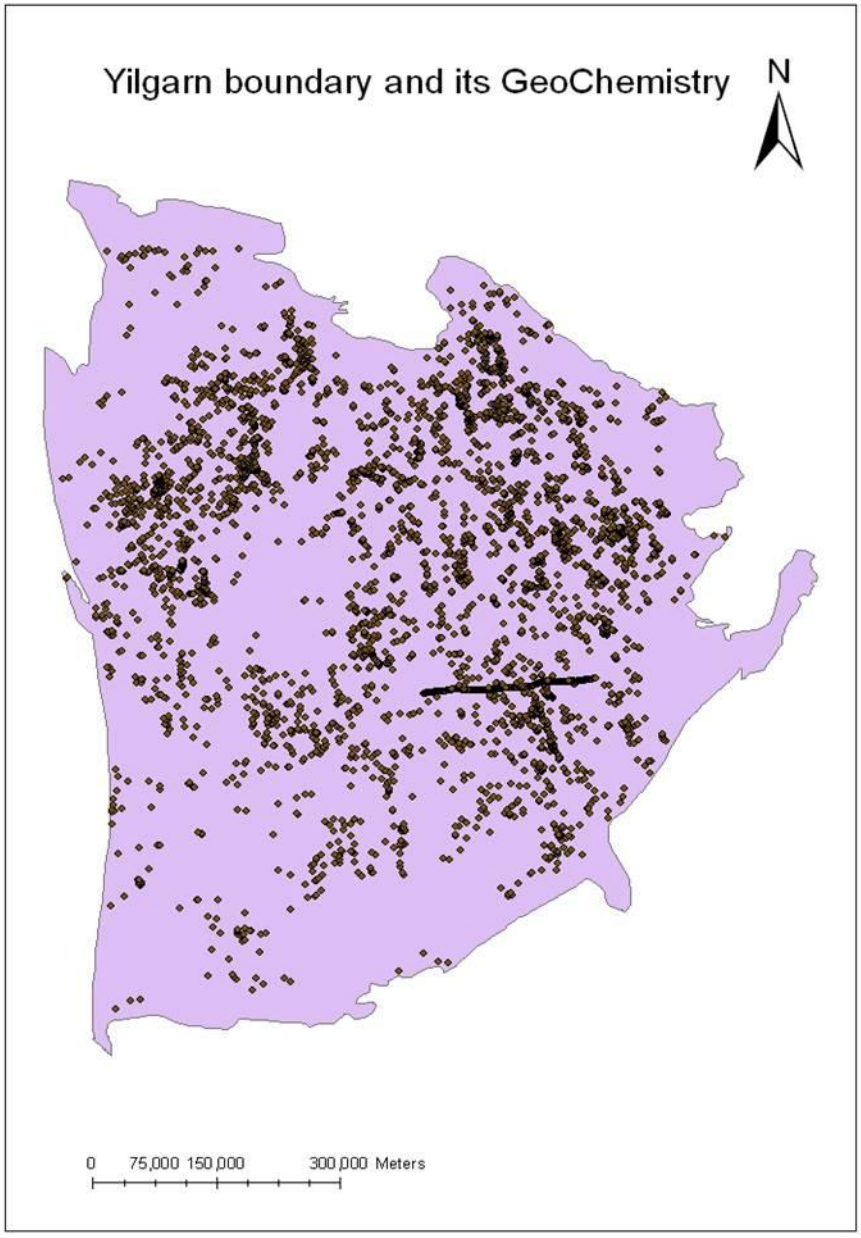

Fig.5 Geochemistry of the study area

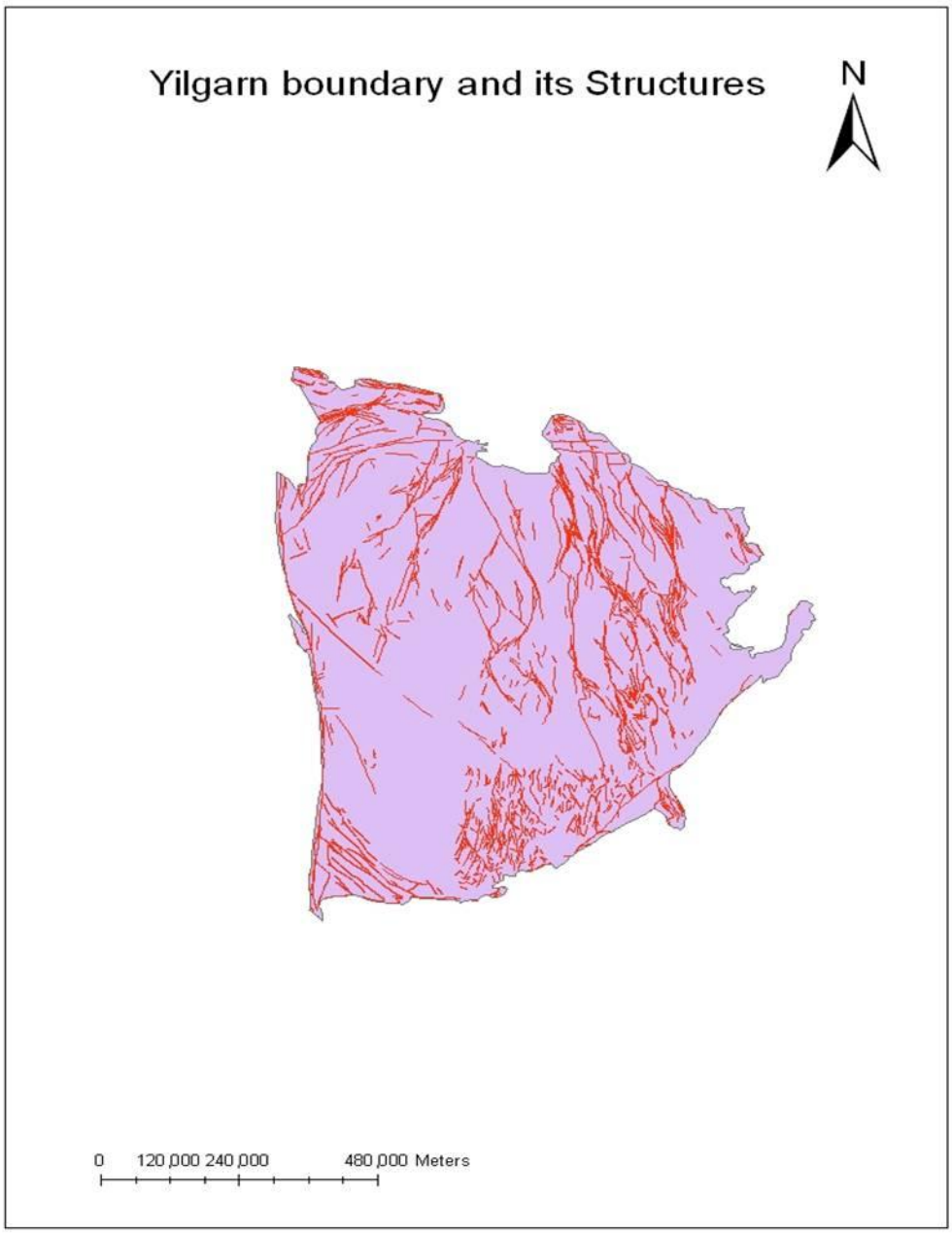

Fig 6 Structure Map of the study area

Several random points were selected and the chemical composition and the rock types at those points were analyzed. The results are associated in the form of attribute tables to each map. Figure 7 explicitly shows the attribute table related to the Geochemistry of the study area respectively.

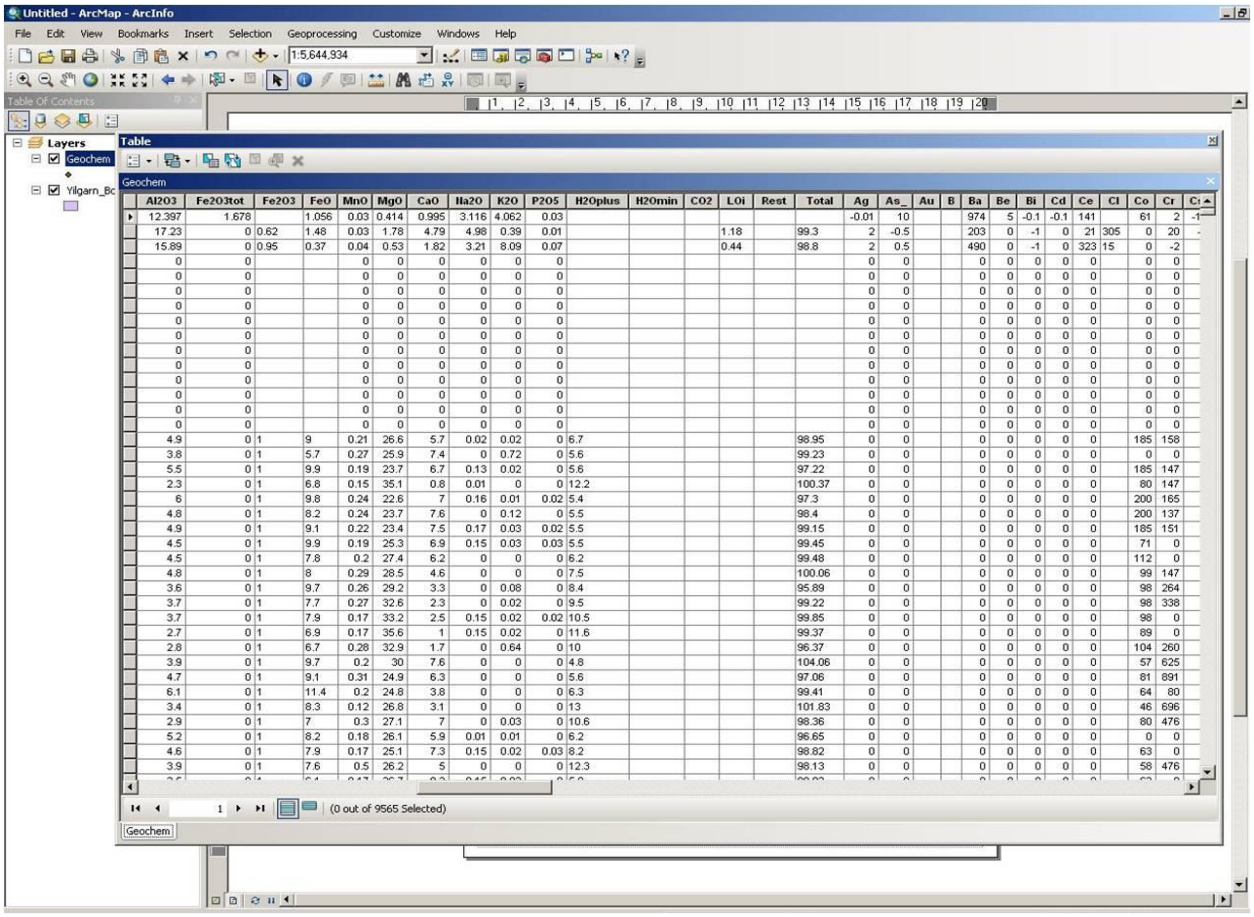

Fig. 7 Attribute table of the Geochemistry of the study area

The procedures used for preparing the above GIS layers are summarized in following table 1.

Predictor Map	**Procedure used for deriving predictor maps**
Geology	Komatiites, Ultramafic rocks, mafic rocks, Sedimentary rocks and other rocks were extracted from bed rock geology data and interpolated using IDW algorithm and reclassified into 5 classes.
Al2O3/TiO2	Ratio of Al2O3 to TiO2 was calculated. The values greater than zero were selected and interpolated using IDW and reclassified into 3 classes 0,1 and 2 whose Al2O3/TiO2 ratios were > 25, <15 and 15-25 respectively.
MgO	From the Geochemistry dataset the values of MgO greater than zero were selected and interpolated using IDW. Finally they were reclassified into 3 classes 0,1 and 2 with MgO values as < 7%, 7%-12% and > 12%.
Proximity to crustal-scale faults	The major faults were extracted from the geology data and buffered to 6 km and reclassified into 6 classes with the distance as 0-1 km, 1-2 km, 2-3 km, 3-4 km, 4-5 km and 5-6 km

Cumulate rocks	Cumulate rocks were selected using spatial query and reclassified into 2 classes 0 and 1 representing the absence and presence of cumulate rocks.
Sulfur anomalies	S values greater than zero were first extracted using the spatial query. The z-scores of those values were calculated and they were interpolated using IDW and reclassified into 10 classes.
Nickel anomalies	The procedure described for sulfur anomalies was followed to prepare nickel anomalies GIS layer.
Chromium anomalies	Chromium anomalies layer used the same procedure as that of sulfur anomalies predictor layer.
Copper anomalies	For the preparation of copper anomalies map, the procedure similar to sulfur anomalies was used.
Crustal contamination	The ratios of La/Sm, La/Yb, Th/Yb, La/Y and Rb/Cs were calculated. For each of those ratios, z-scores were estimated. IDW algorithm was used for interpolation and reclassified into 10 classes.

TABLE 1: Methods used to prepare the different Predictor Maps

6.3 Favourable Geological Settings and Pathways

Greenstone belts, which include extensive komatiite sequences, compromise the favourable geological setting for magmatic nickel sulfide deposits in the Yilgarn Craton and were used as the study area for the prospectivity analysis. Crustal-scale faults in the Yilgarn Craton have a close spatial and genetic association with the known nickel sulfide deposits and are considered potential pathways for the intruding magma to reach higher levels of the crust therefore promoting crustal contamination, sulfur saturation and segregation of nickel sulfide to form ore deposits at mineable depths. A predictor map showing proximity to crustal-scale faults was used as proxy for potential pathways for ascending source magmas. Table 1 summarizes the procedure used for obtaining the map

6.4 Sulfur Saturation

Nickel is a chalcophile element which partitions into sulfide phase. Magmatic nickel sulfide deposits form due to saturation of nickel-rich, mantle-derived, mafic and ultramafic magmas with respect to sulfur, which results in formation and segregation of immiscible nickel sulfide liquid. Geochemical proxies are routinely applied as direct exploration tools for inferring sulfur saturation (e.g., Naldrett, 1977; Brand, 1999; Barnes et al., 2004; Lightfoot, 2007).

In this analysis, the following predictor maps were prepared whose procedures are mentioned in Table 1

- Cumulate rocks indicating fractionation
- S anomalies indicating potential sulfur sources
- Cu, Ni and Cr anomalies indicating fertility of metals and occurrence of nickel extraction extraction processes and
- Crustal contamination of the melt during emplacement as indicated by anomalous incompatible element ratios such as La/Sm, La/Yb, Th/Yb, La/Y and Rb/Cs. The greater the crustal contamination of the melt during emplacement, the higher the values of the above ratios.

By the end of these processes, ten different predictor layers were obtained, which are shown from figures 8 to figure 17.

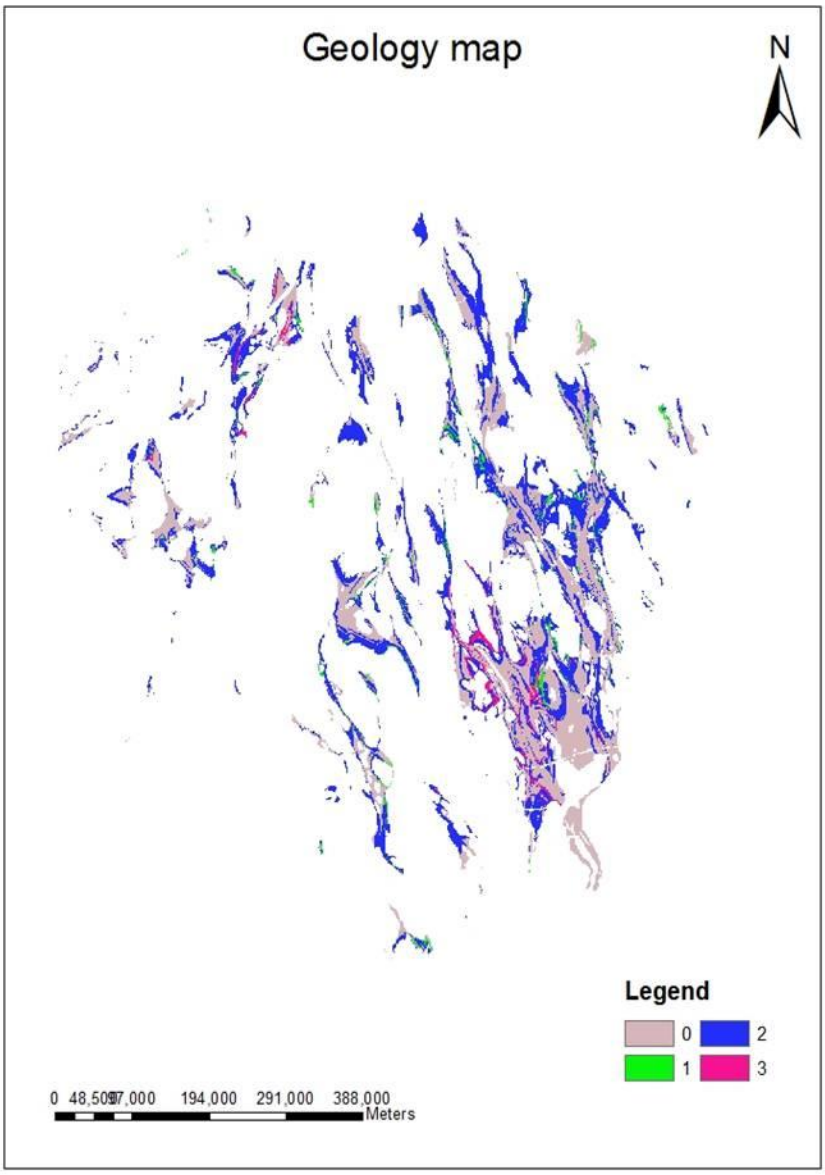

Fig 8. Geology Map of the study area where 0, 1, 2 and 3 represent Sedimentary rocks, Mafic Rocks, Ultra-mafic rocks and komatiites respectively.

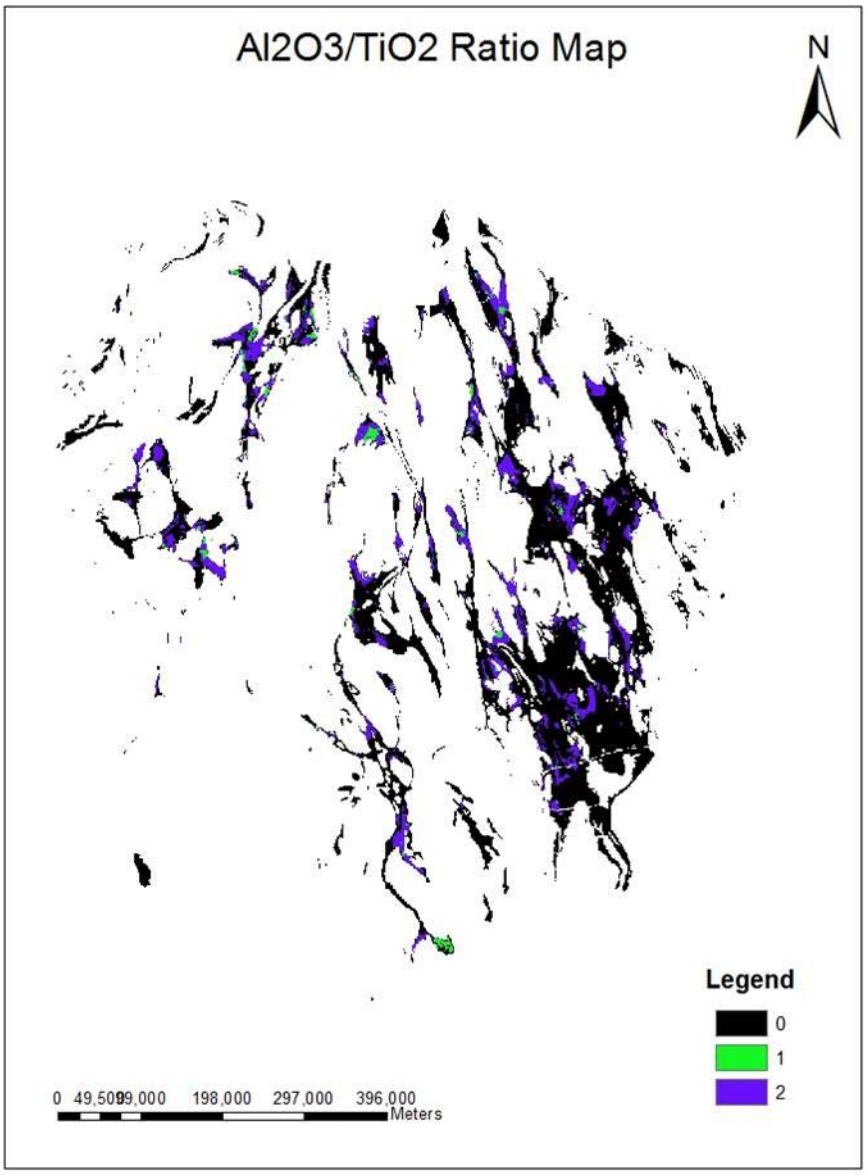

Fig 9. Al2O3/TiO2 ratio of the study area where 0, 1 and 2 represent Al2O3/TiO2 > 25, Al2O3/TiO2<15 and Al2O3/TiO2 between 15-25 respectively.

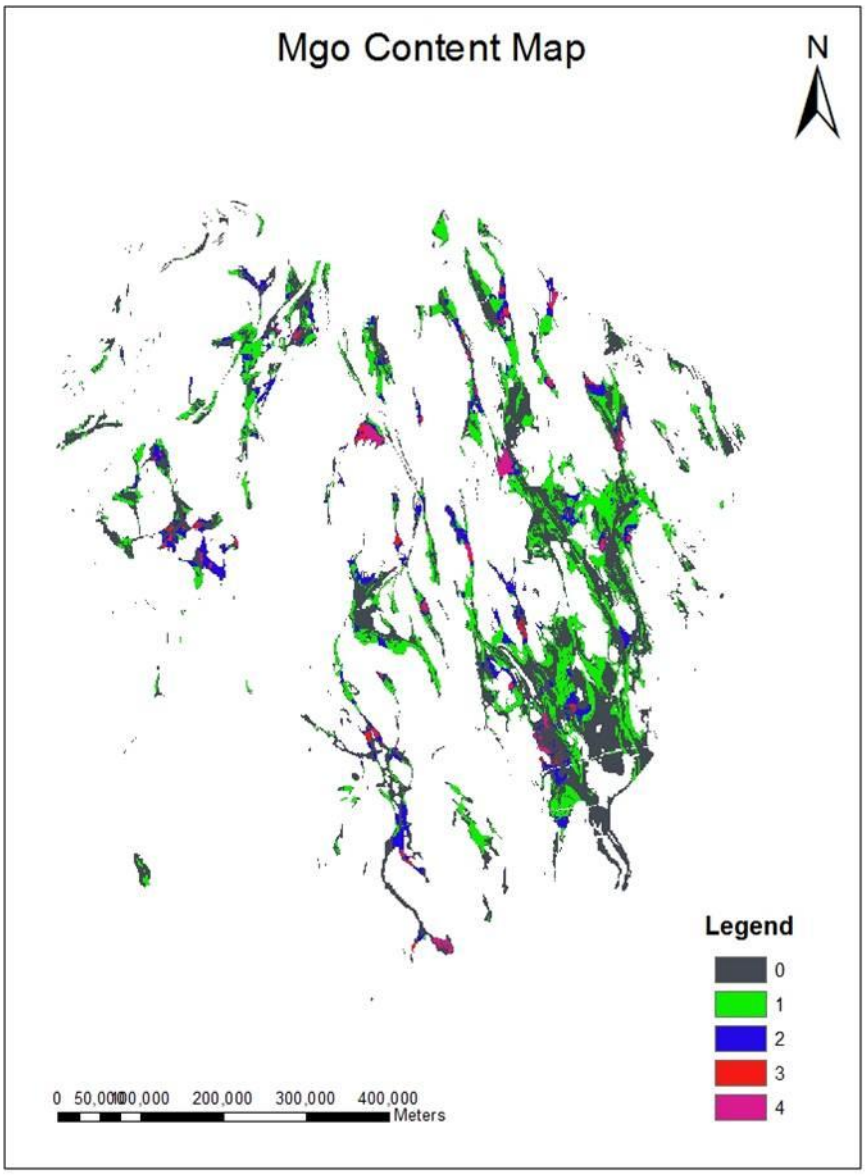

Fig10 MgO content map of the study area where 0 & 1 represent MgO value < 7%

2, 3 represent MgO value between 7% to 12% & 4 represents MgO value > 12%

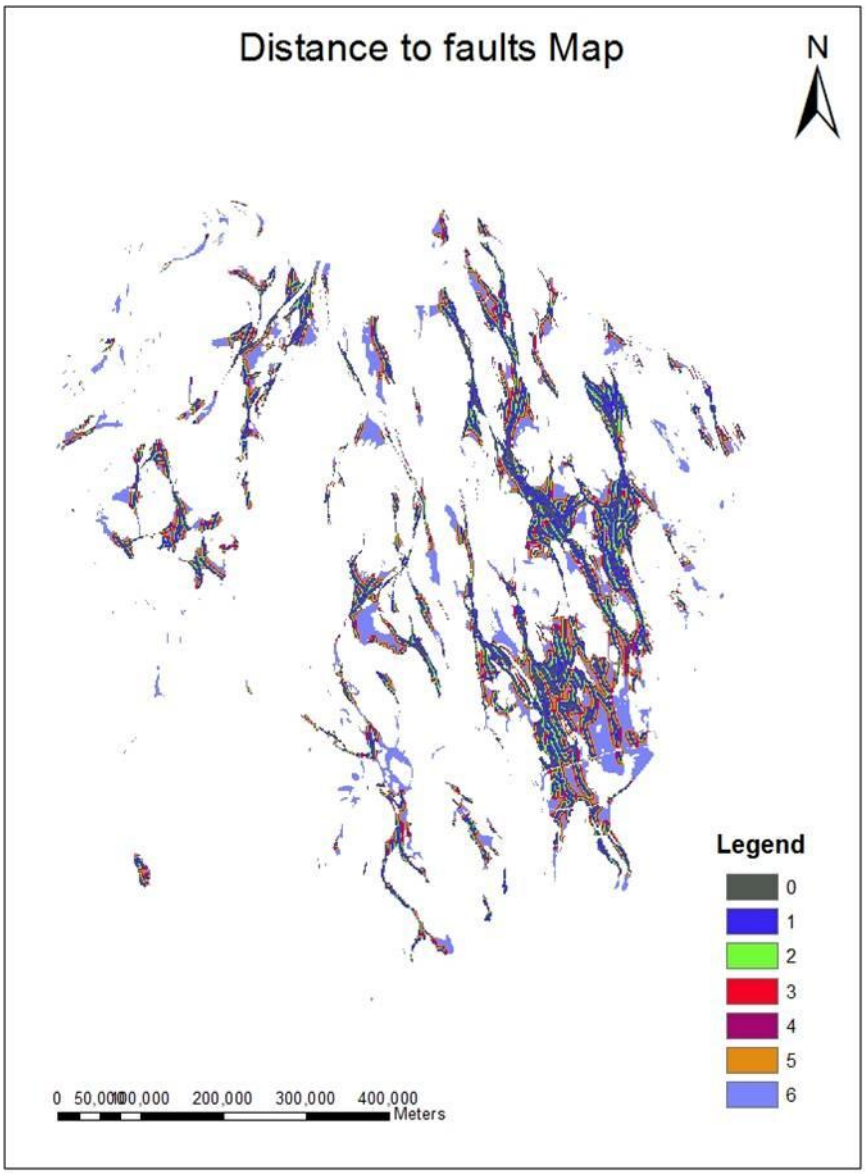

Fig 11 Map showing the distances to the faults in the study area where 0, 1, 2, 3, 4, 5 and 6 represent distances 0-1 km, 1-2 km, 2-3 km, 3-4 km, 4-5 km and 5-6 km respectively.

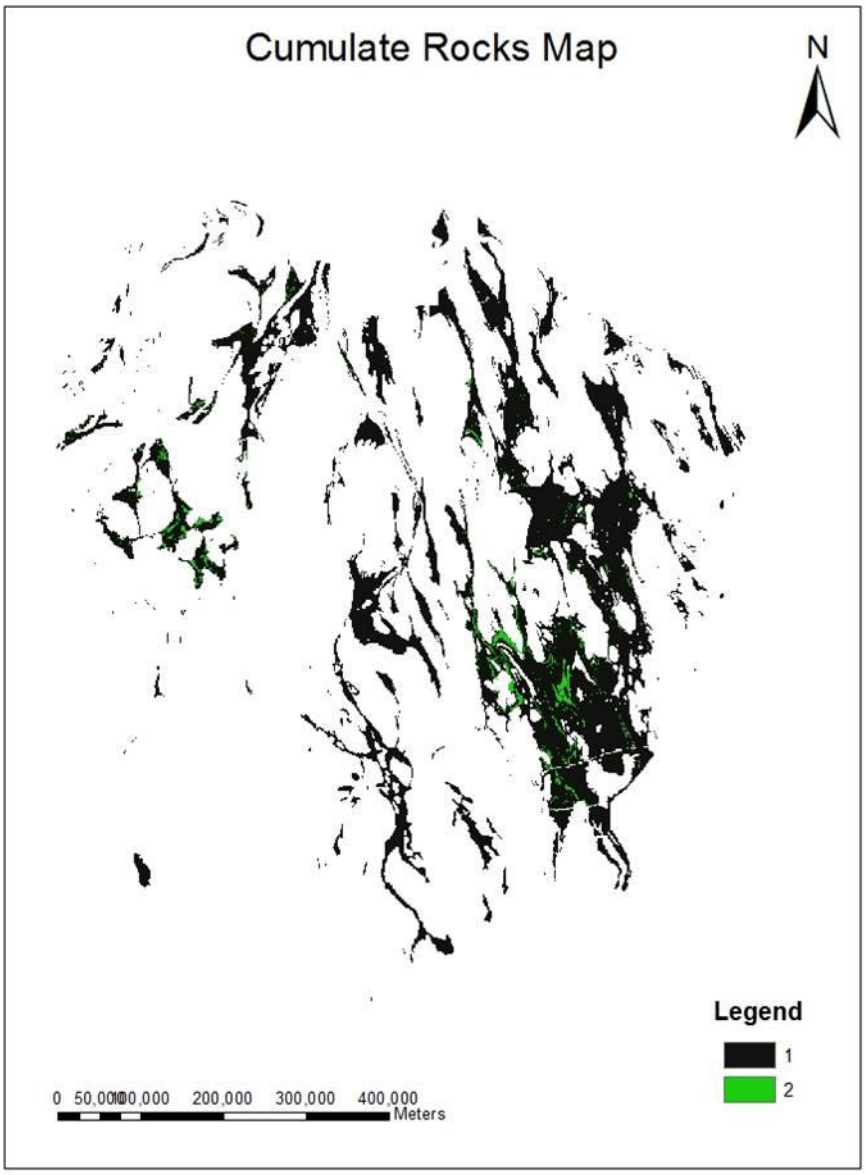

Fig 12 Cumulate rocks Map of the study area where 1 indicates the absence and 2 indicates the presence of cumulate rocks.

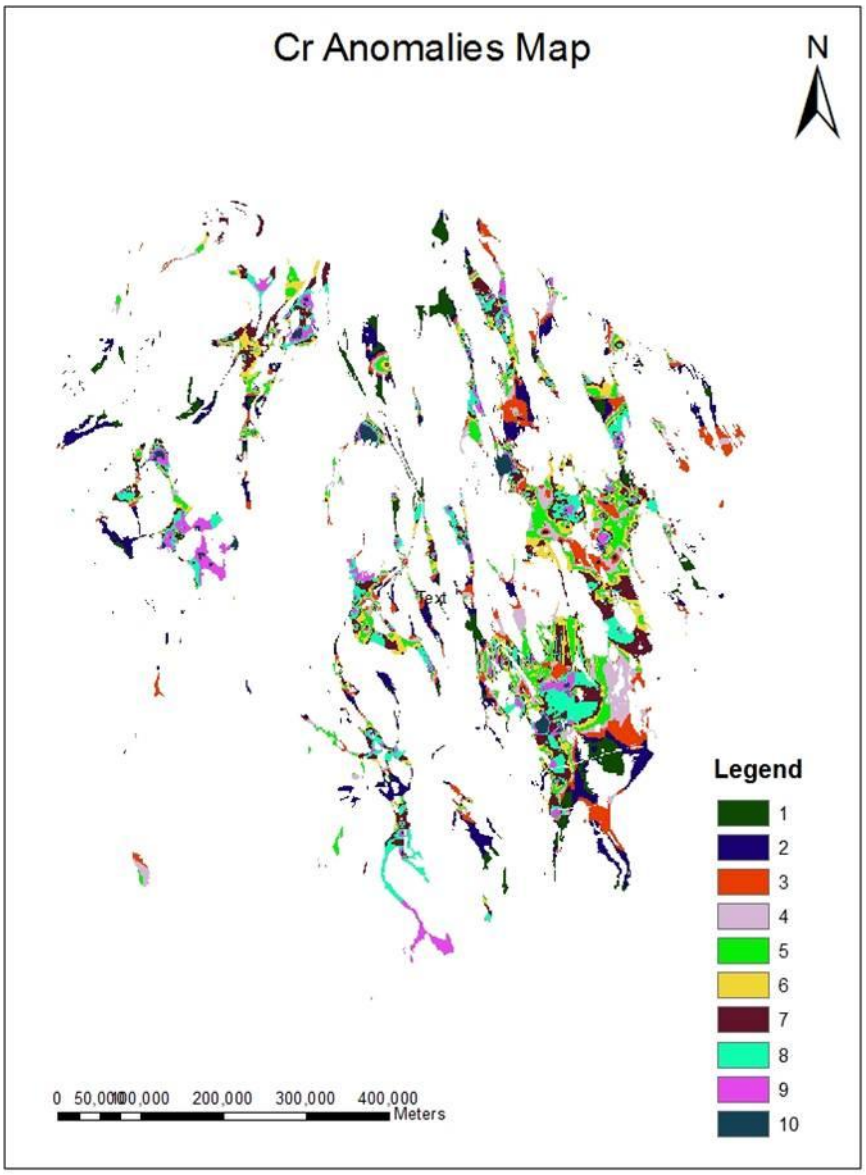

Fig 13 Chromium Anomalies Map of the study area where values 1 to 10 indicate the reclassified values of Cr anomalies in the ascending order

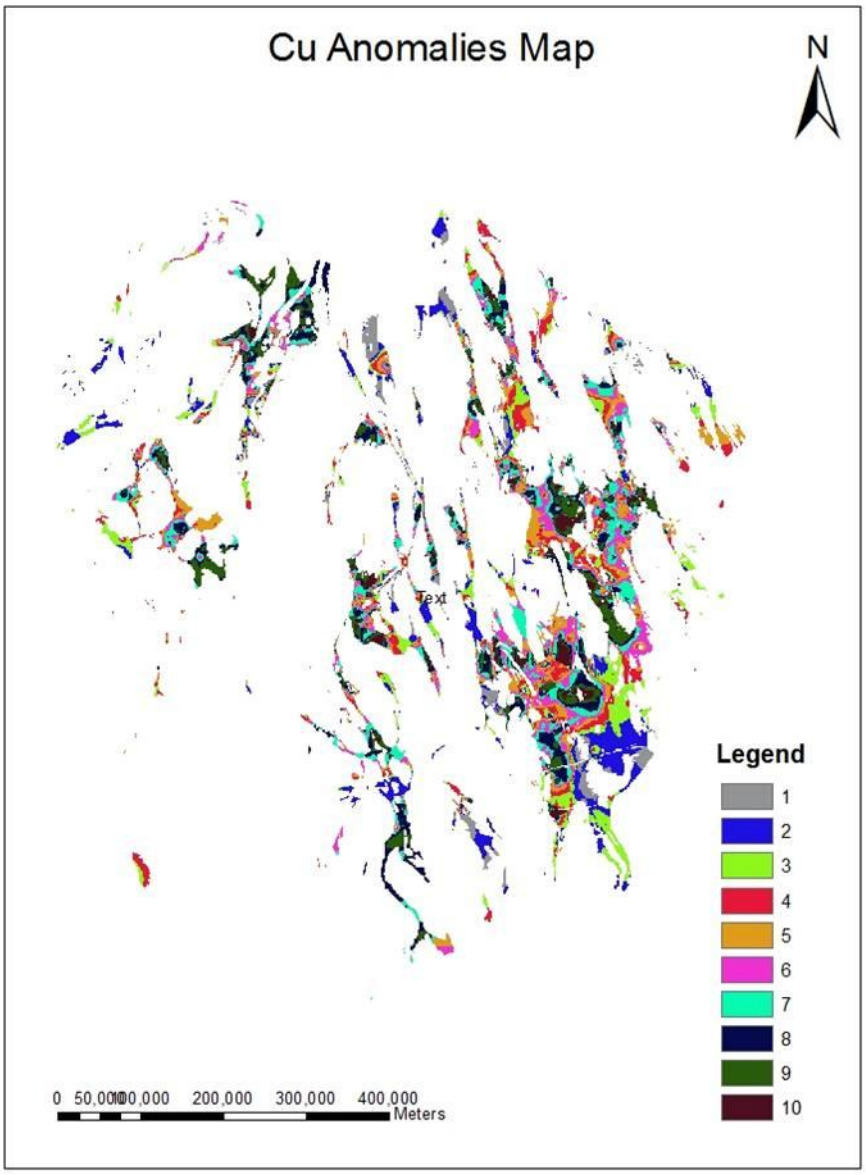

Fig 14 Copper Anomalies Map of the study area where values 1 to 10 indicate the reclassified values of Cu anomalies in the ascending order

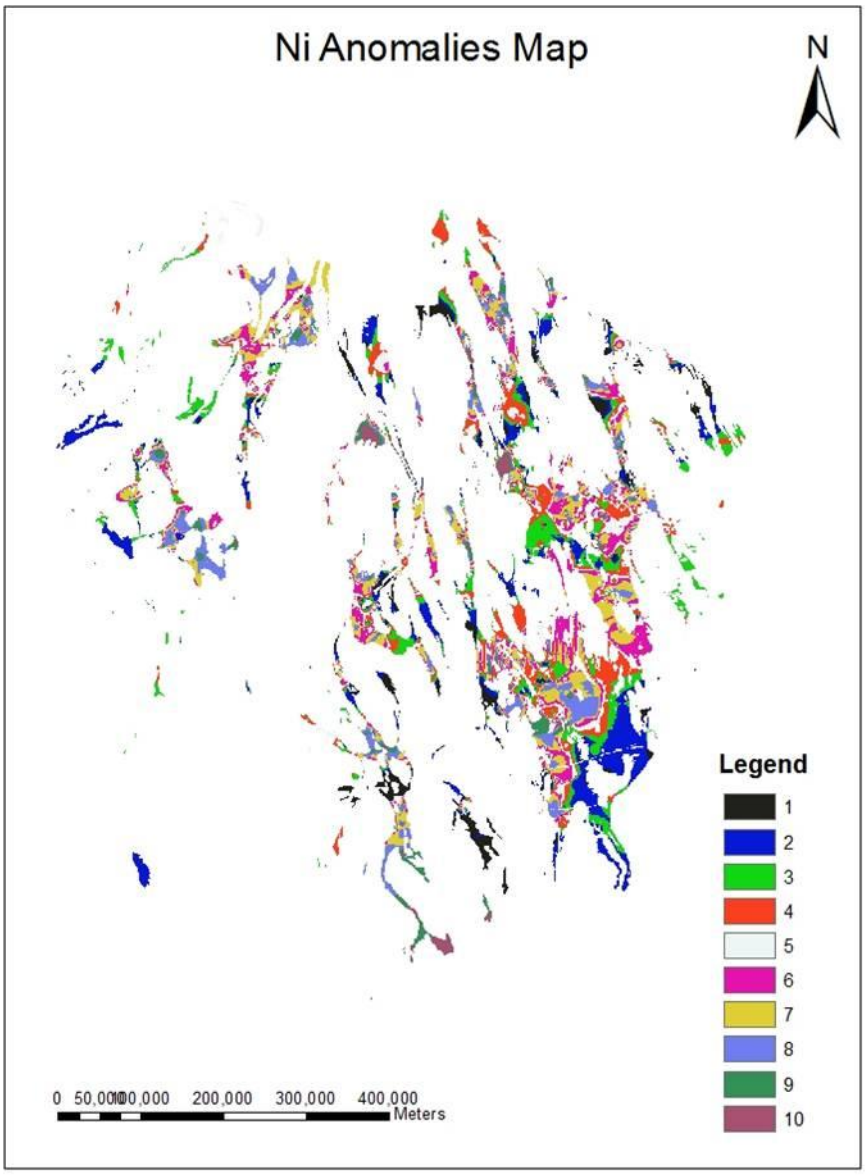

Fig 15 Nickel Anomalies Map of the study area where values 1 to 10 indicate the reclassified values of Ni anomalies in the ascending order

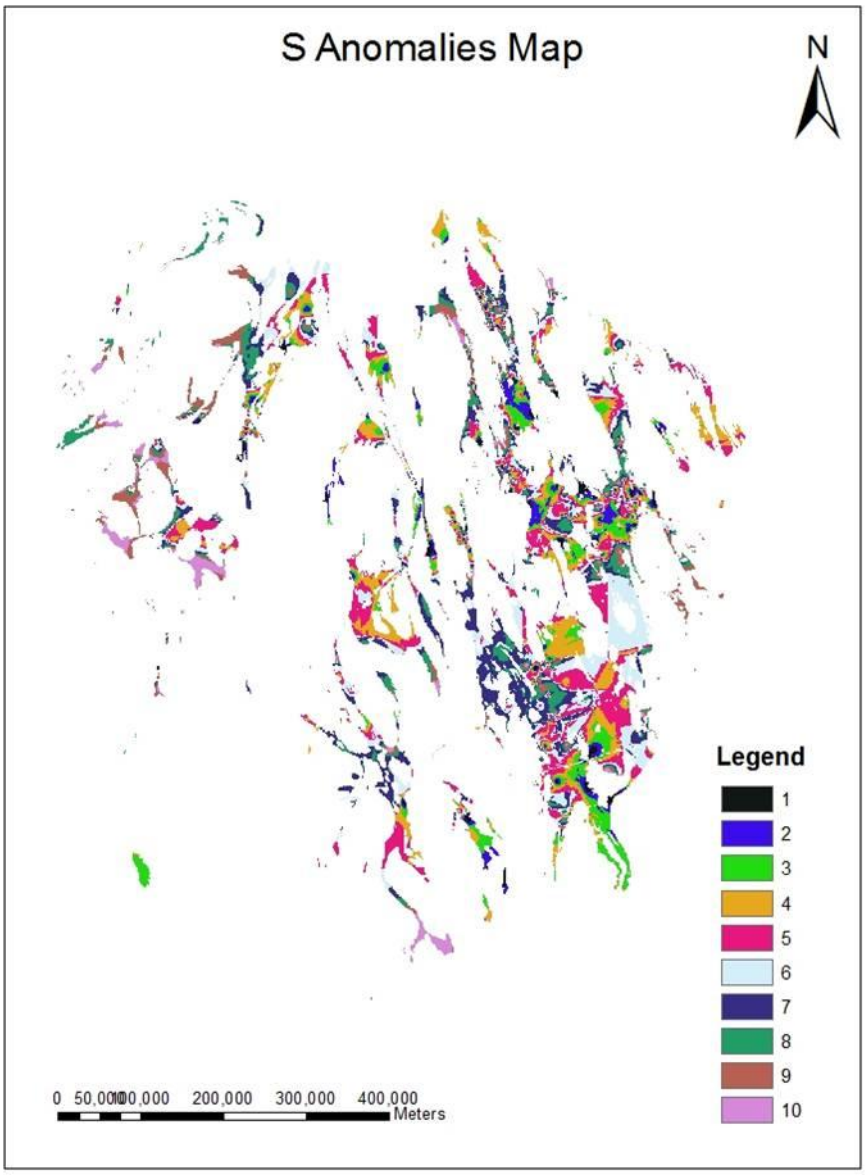

Fig 16 Sulphur Anomalies Map of the study area where values 1 to 10 indicate the reclassified values of S anomalies in the ascending order

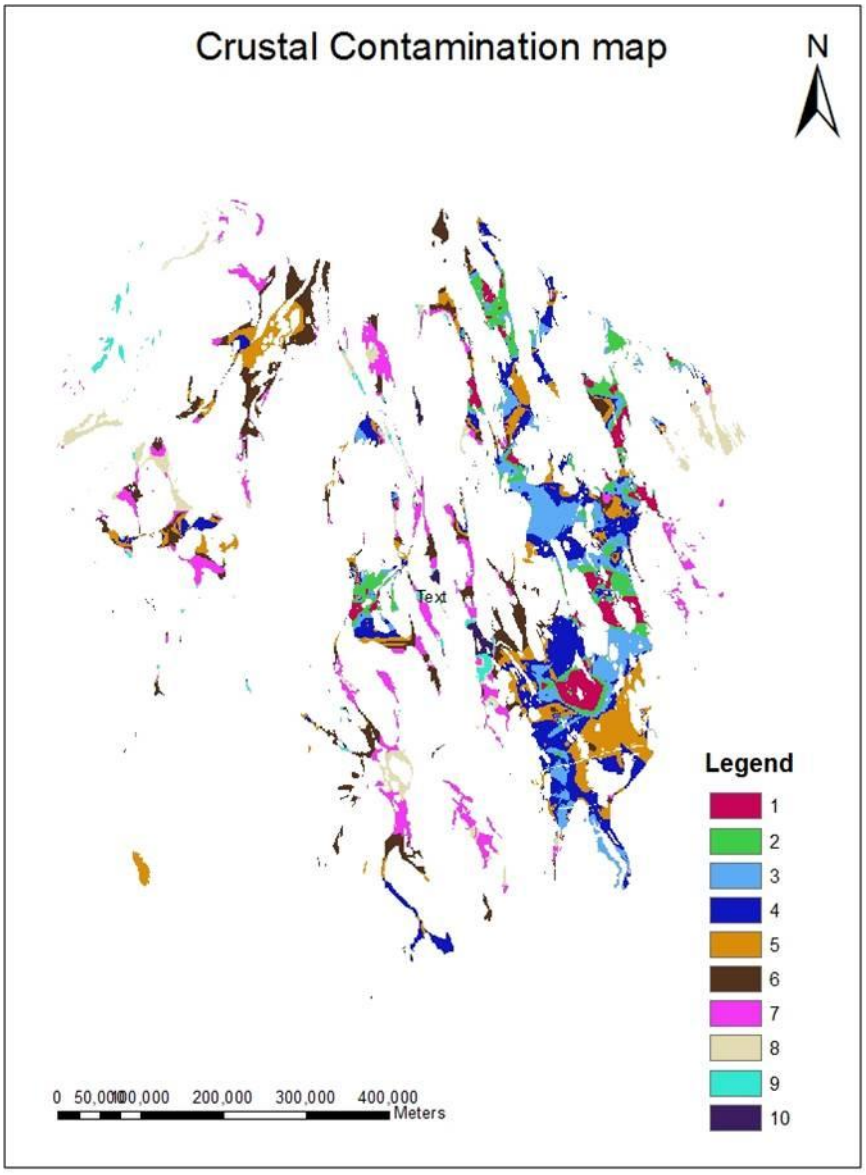

Fig 17 Crustal Contamination Map of the study area where values 1 to 10 indicate the reclassified values of crustal contamination in the ascending order

6.5 Preparation Of Training, Validation and Classification Datasets

Having 163 known nickel deposits in the Yilgarn Craton, 170 points were created randomly. These two datasets form the 'Training Points' and was used to prepare the validation, training and classification datasets for each of the three exploration criteria. The three exploration criteria GIS layers were combined to form one single predictor layer whose training, validation and classification datasets were also prepared.

6.5.1 Training Points Creation

170 random points were created within the study region representing the 'Non-deposit Data'. These together with the 163 known deposits form the 'Training points'. A field named 'code' is created in the both known deposit data and non-deposit data set. A value of 0 and 1 was assigned to the field 'code' to the non-deposit and known deposit data set respectively.

6.5.2 Unique Combination Grid

A Unique Combination Grid (UCG) for each of the exploration criterion was created which represented the 'Classification Dataset'. The 'training points' were used to extract the training and validation datasets from the UCG. 70% of the datasets extracted from each of the UCGs using training points were used as 'Training Data' and the rest

30% were used as ‘Validation Data’. Figure 18 shows the training points selected for this purpose and figure 19 shows the attribute table of the training points.

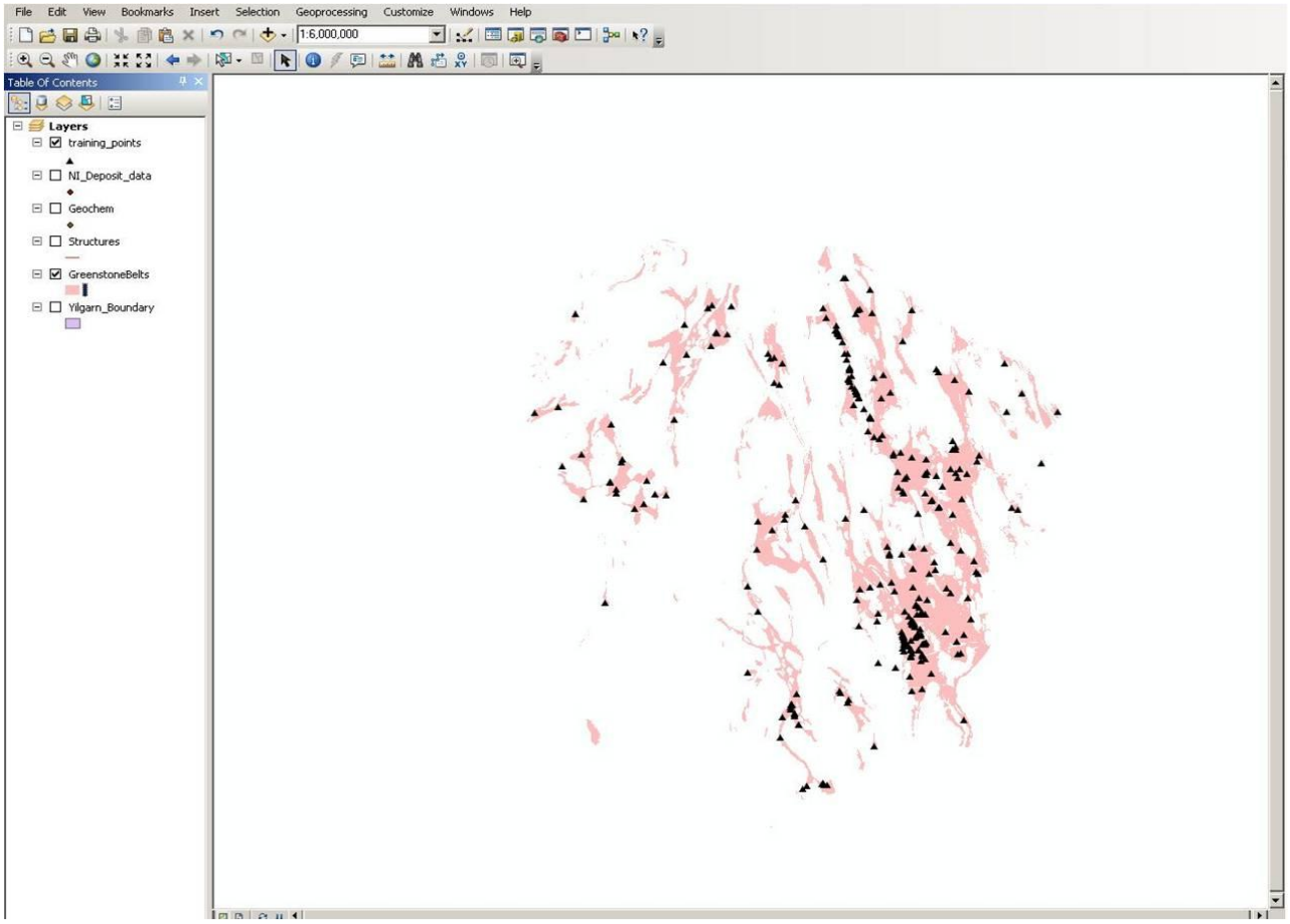

Fig 18 ArcGIS window showing the Greenstone Boundary and the training points

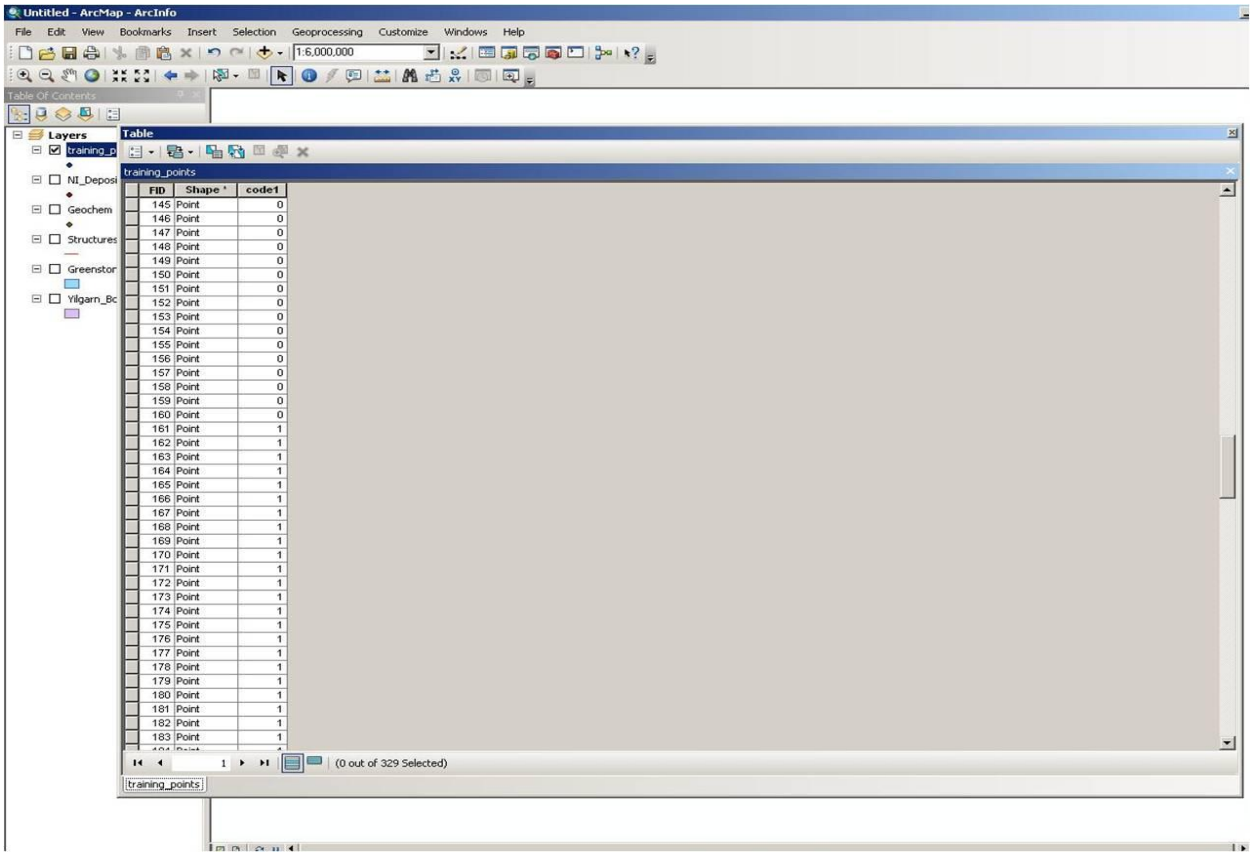

Fig 19 Attribute table of the training points

Once the ten different predictor maps are prepared, there are combined to three different maps based on the exploration criteria. Thus the Geology, Al2O3/TiO2 ratio and MgO content maps are combined to form the source maps. The figures 20 and 21 represent the source map and its corresponding attribute table.

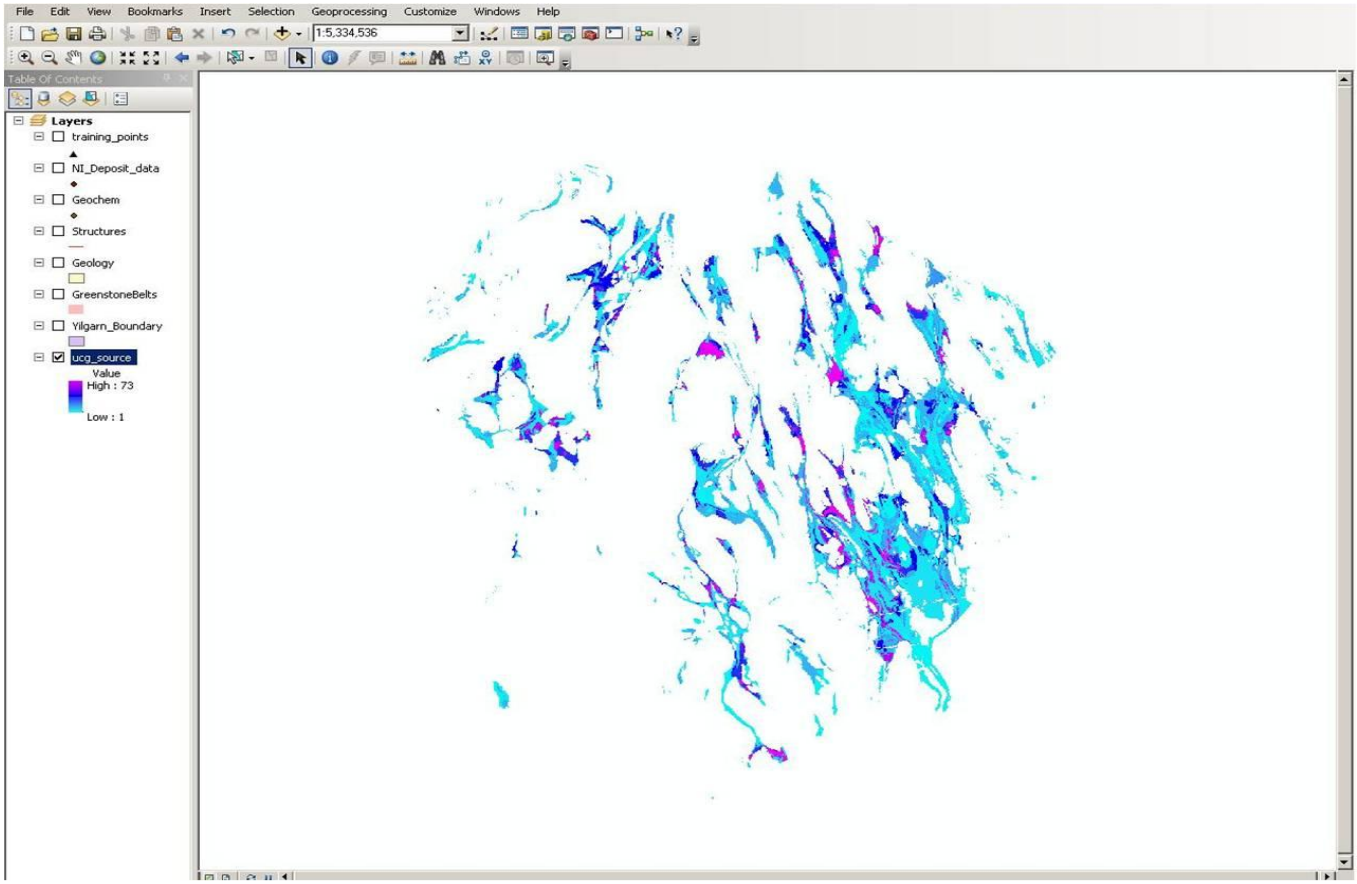

Fig 20 ArcGIS window showing the source map which is the combination of Geology, Al2O3/TiO2 ratio and MgO content maps

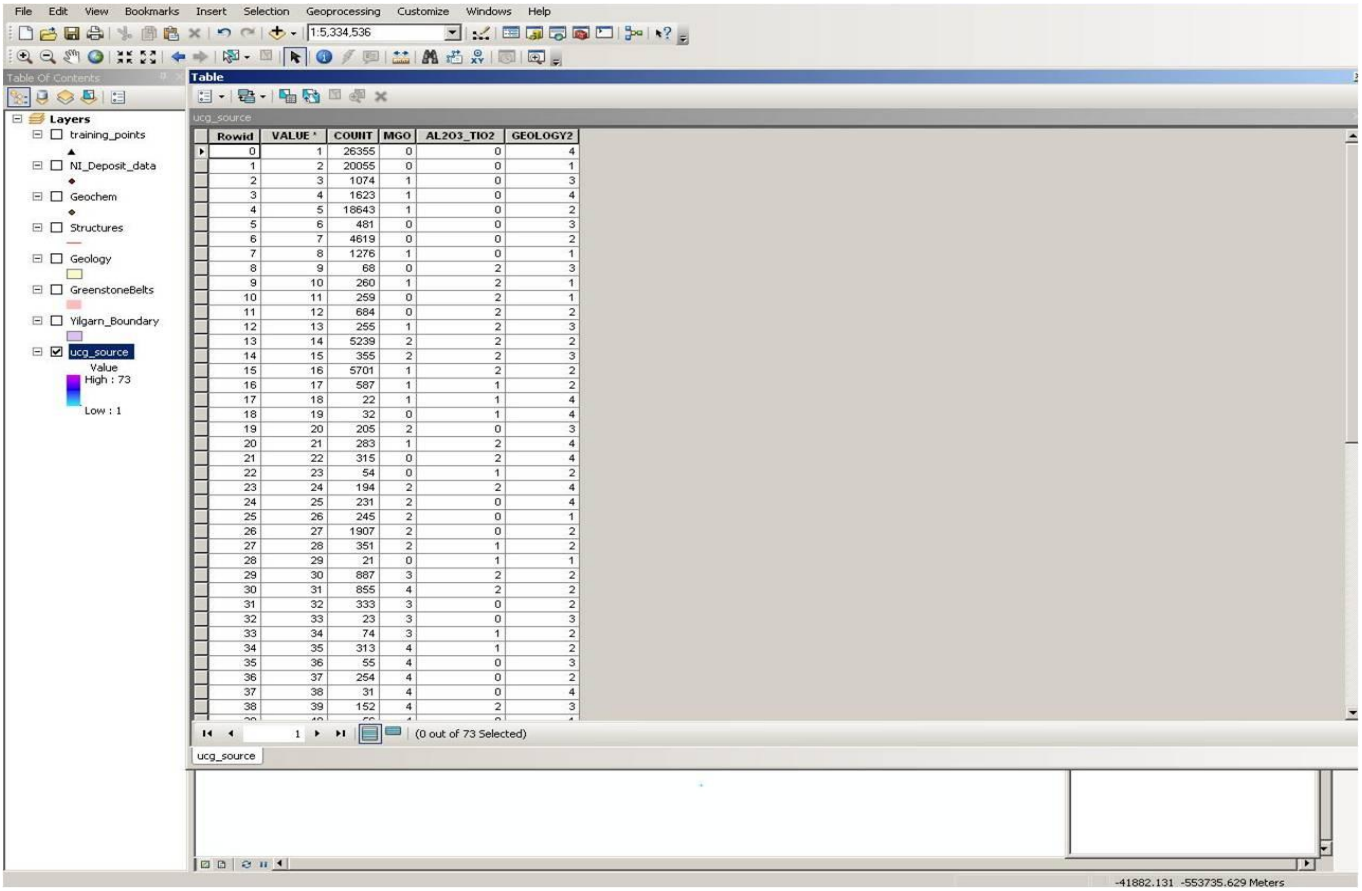

Fig 21 Attribute table of the source map showing the values of each exploration criterion

Similarly, the distance to faults map is obtained and the figure 22 depicts the map and the figure 23 shows its related attribute table.

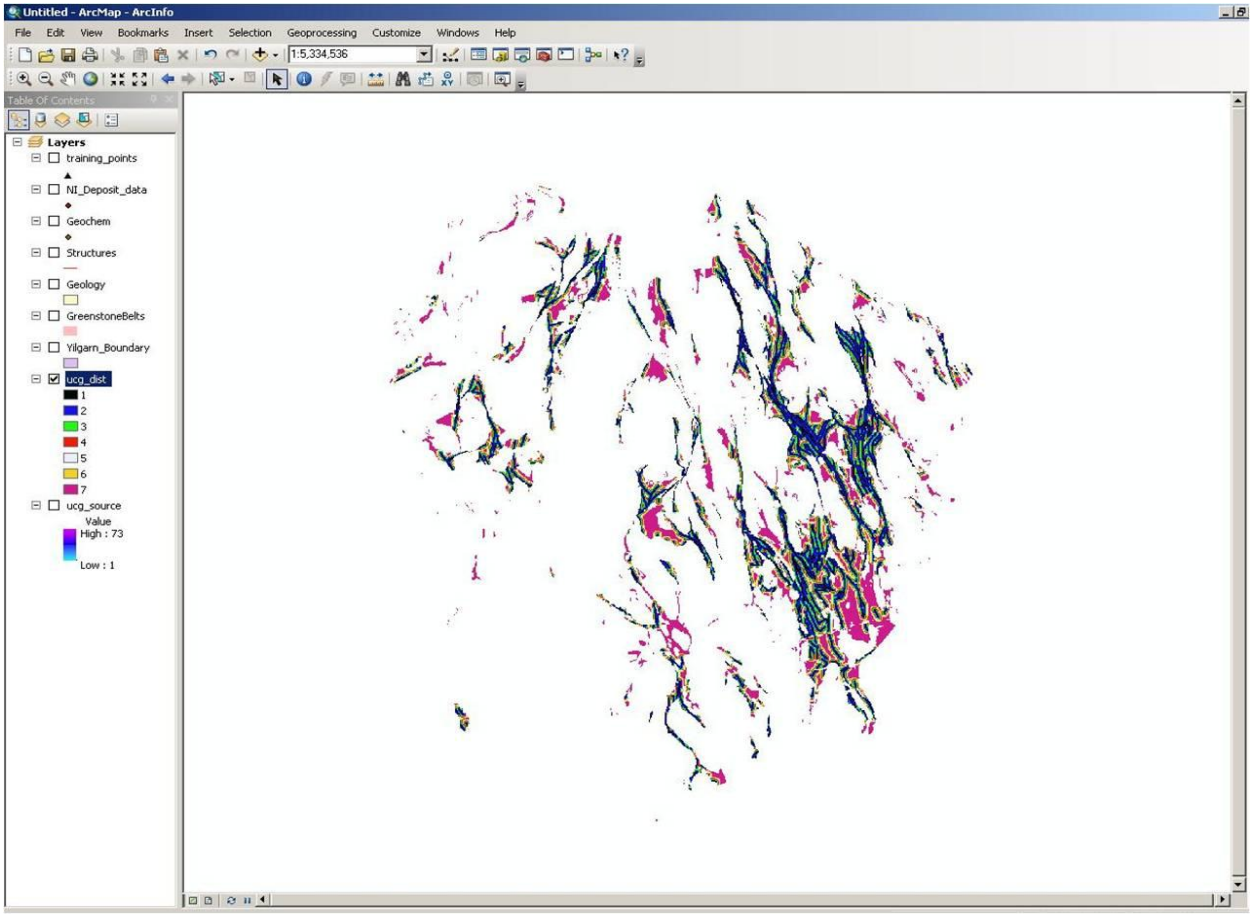

Fig 22 ArcGIS window representing the distance to the faults

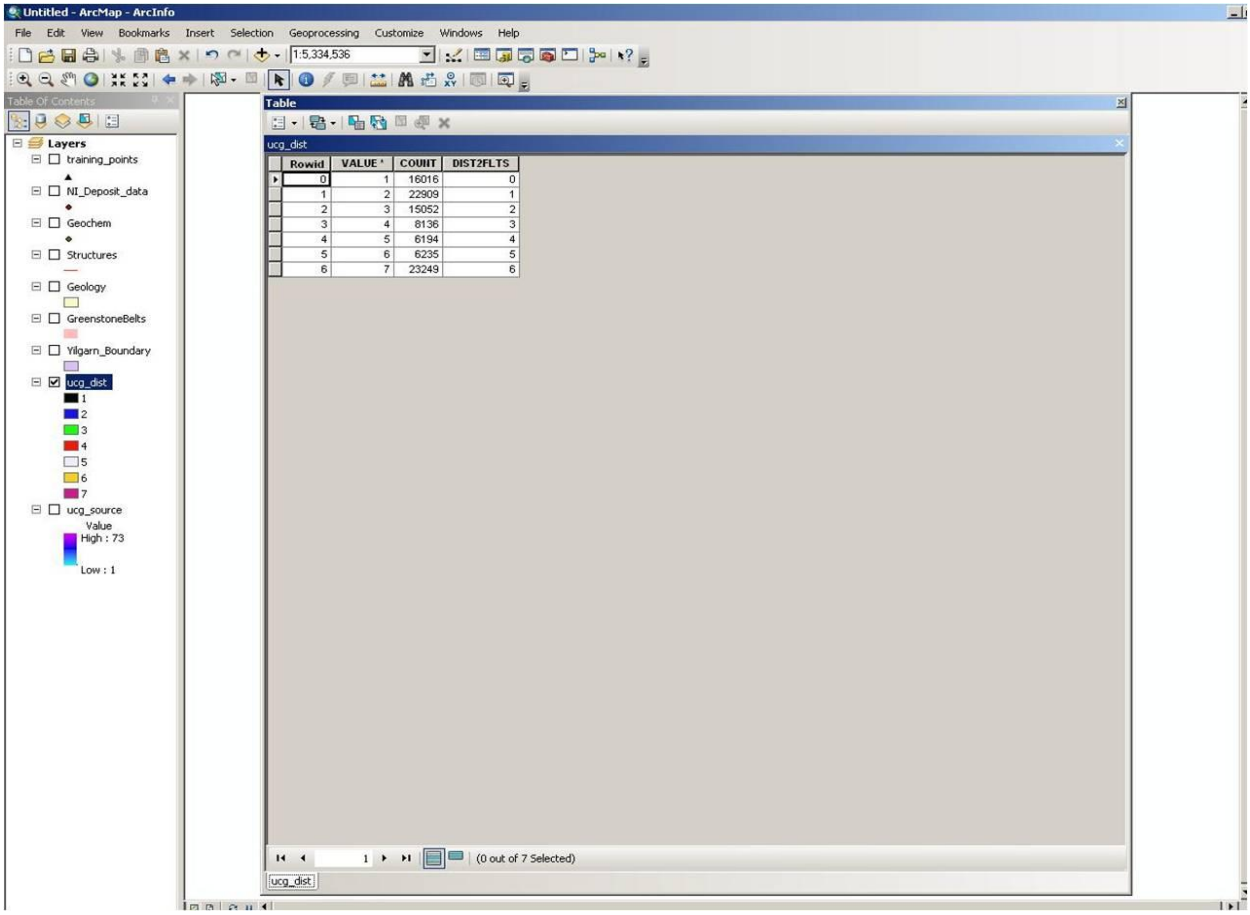

Fig 23 Attribute table of the distance to faults map

Likewise the anomalies maps are combined to form the sulphur saturation map which is depicted in the figure 24 and figure 25 shows the attribute table associated with it.

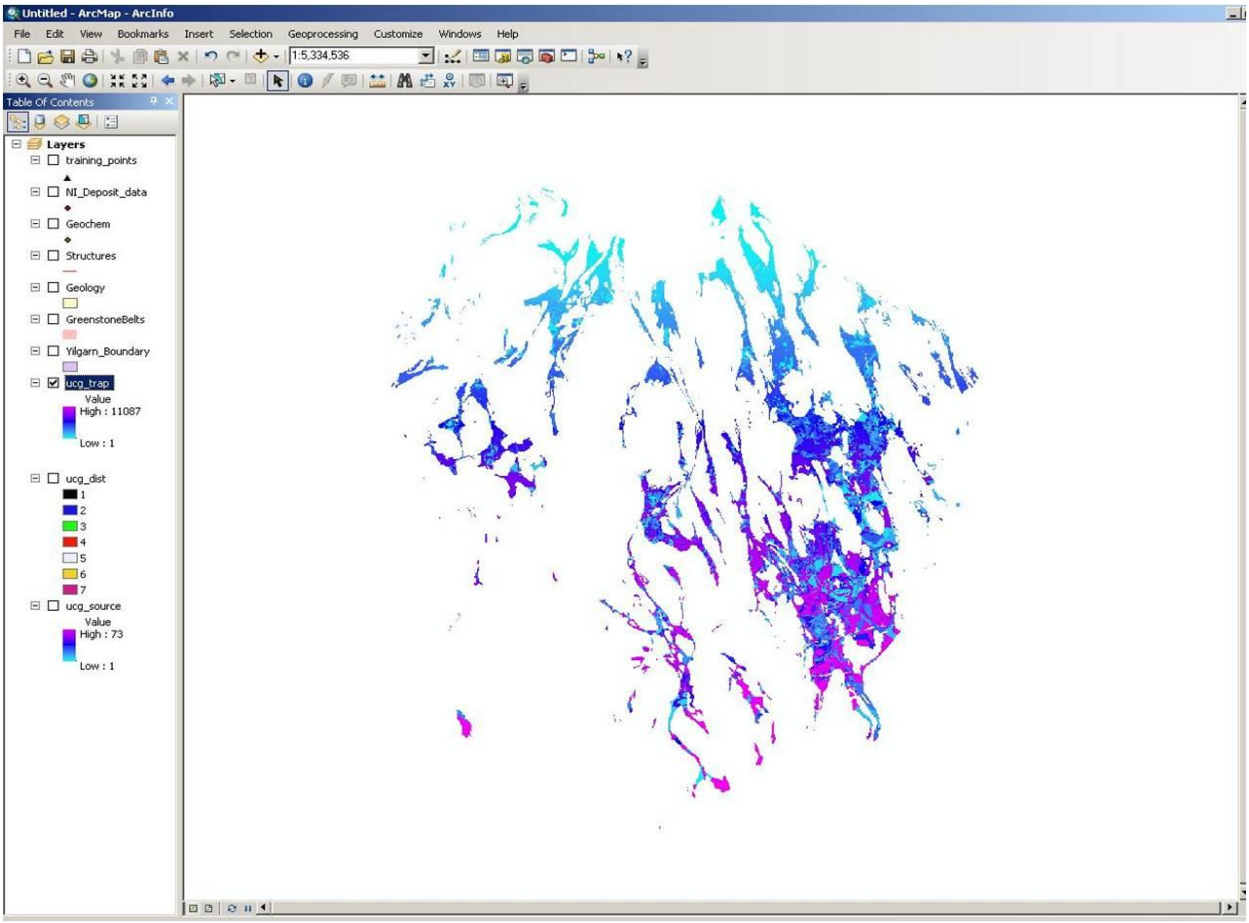

Fig 24 ArcGIS window showing the sulphur saturation in the Greenstonebelt region

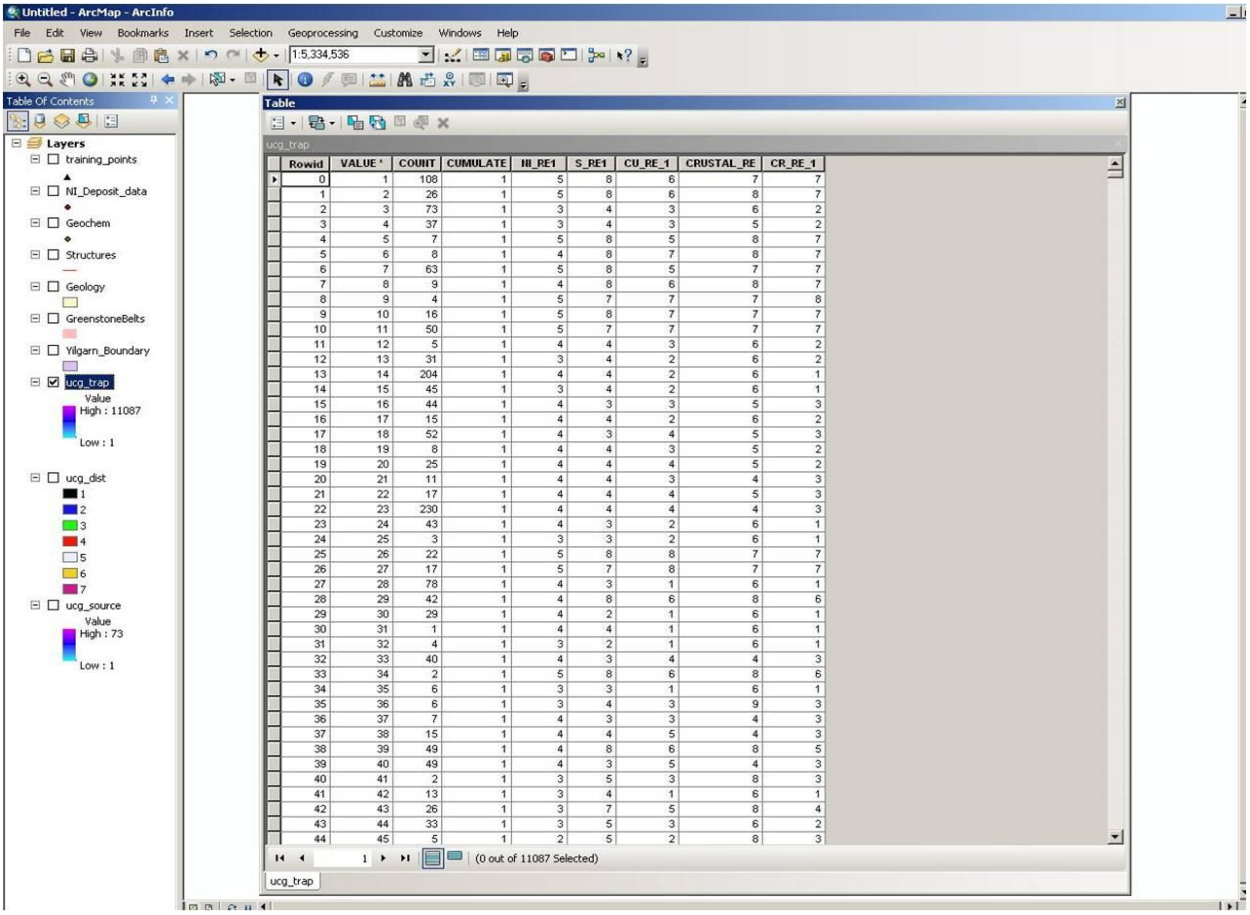

Fig 25 attribute table of the trap showing various anomalies

Finally all these three exploration criteria maps are combined to form a single one and is shown in figure 26

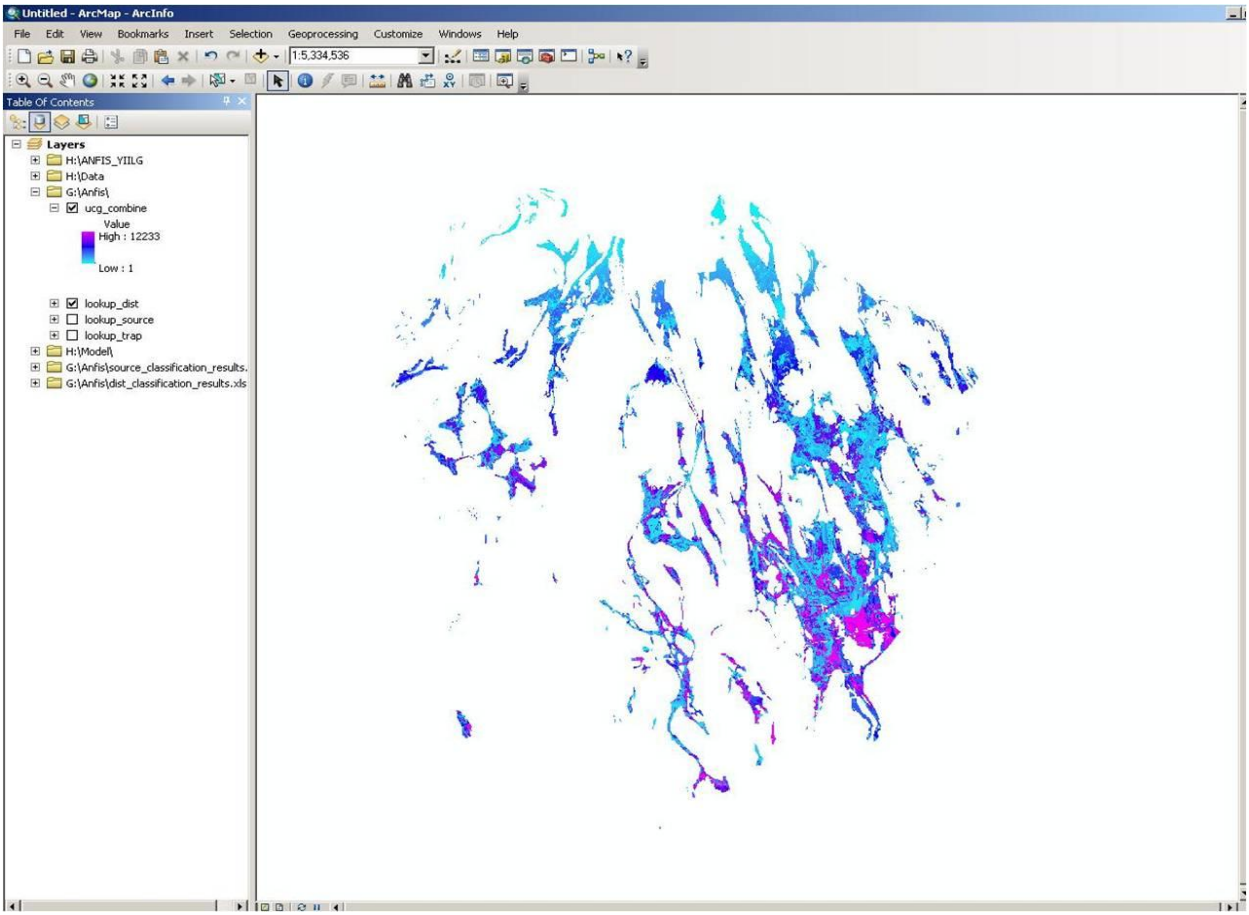

Fig 26 ArcGIS window representing the combination of all the three exploration criteria

The corresponding attribute table is shown in the figure 27.

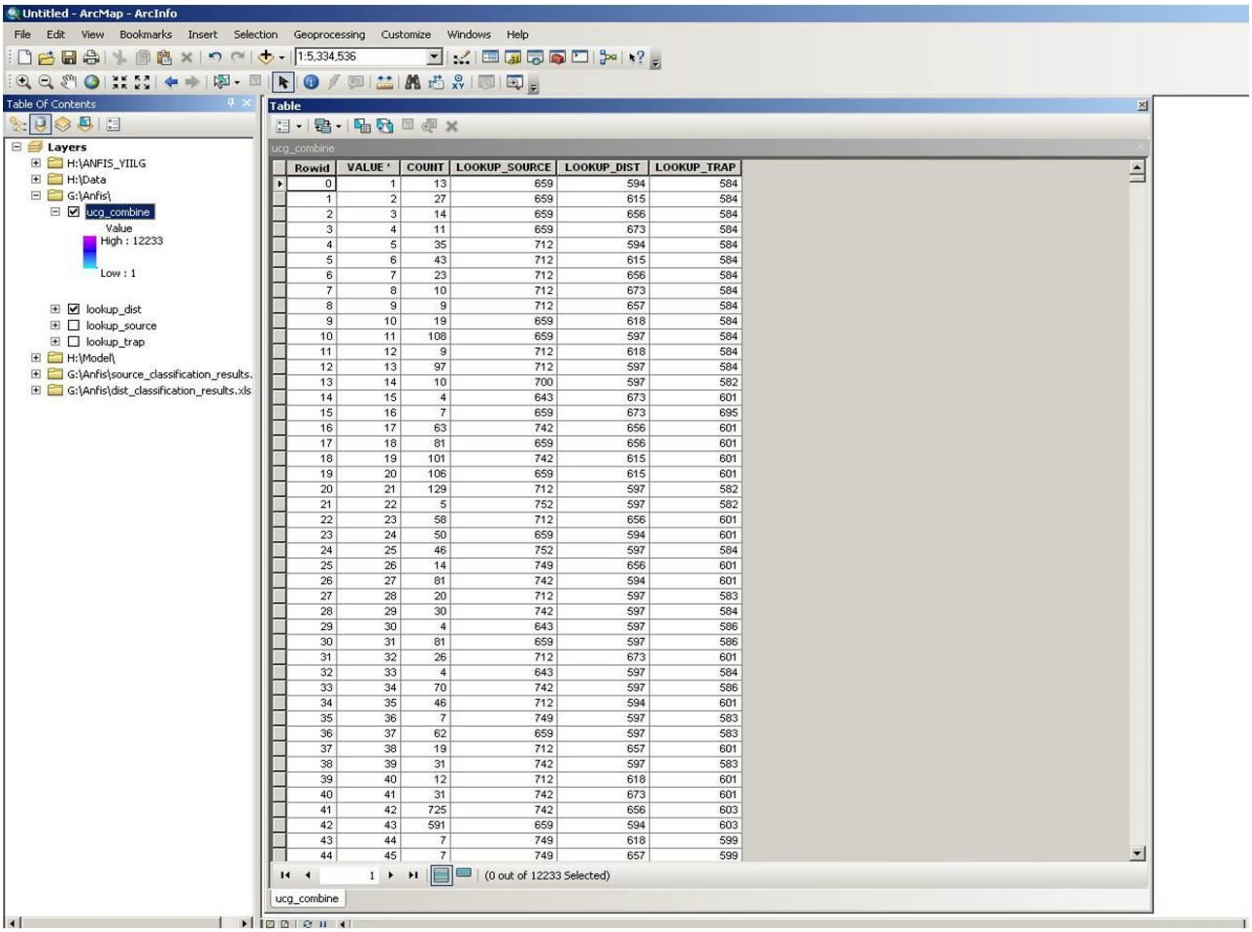

Fig 27 Attribute table of the combined exploration criteria

7. ADAPTIVE NEURO FUZZY MODELING OF MAGMATIC NICKEL SULFIDE SYSTEMS IN THE YILGARN CRATON

7.1 Mamdani and Sugeno types

A fuzzy inference system simulates human cognition in modeling the conceptual component of information by employing fuzzy membership functions and fuzzy if-then rules. Several fuzzy inference systems have been described by different workers (Zadeh, 1973; Mamdani, 1974; Mamdani and Assilian, 1975; Tsukamoto, 1979; Takagi and Sugeno, 1985; Sugeno and Kang, 1988; Sugeno and Tanaka, 1991) but the most commonly-used are Mamdani type (Mamdani, 1974; Mamdani and Assilian, 1975) and Takagi-Sugeno type, which is also known as Takagi-Sugeno-Kang type (Takagi and Sugeno, 1985; Sugeno and Kang, 1988; Sugeno and Tanaka, 1991). In the case of a Mamdani type fuzzy inference system, both premise (if) and consequent (then) parts of a fuzzy if-then rule are fuzzy propositions. In the case of a Takagi-Sugeno type fuzzy inference system, where the premise part of a fuzzy rule is a fuzzy proposition, the consequent part is a mathematical function, usually a zero or first degree polynomial function.

7.1.1 Takagi Sugeno type of FIS

The hybrid neuro-fuzzy model for mineral potential mapping described here is a Takagi-Sugeno type fuzzy inference system, which is implemented in the framework of adaptive neural networks. It is an adaptation of "adaptive network- based fuzzy inference system" (ANFIS; Jang, 1993) for mineral potential mapping.

7.1.2 Fuzzy Membership Values

One of the most significant procedures in hybrid neuro-fuzzy modeling is the definition of fuzzy membership values. The Gaussian fuzzy membership functions return membership values that lie between 0 and 1. However, fuzzy membership values returned by these functions are determined by the values of the parameters c and _, which, respectively, define the center and the spread of the functions. Because the fuzzy membership values propagate through a model and control the final output, it is important to estimate the values of these parameters precisely.

Porwal et al. (2003a) used a similar Gaussian function for calculating fuzzy membership values in the knowledge-driven fuzzy model for mineral potential mapping. However, a fuzzy model does not possess a learning capability and therefore the values of parameters of the function were estimated

heuristically. Neural networks, on the other hand, possess an excellent capability of learning from empirical data and therefore the implementation of fuzzy model in the framework of adaptive neural networks provides a more efficient method for parameter estimation.

However, a large number of fuzzy sets results in an undesirably large number of model parameters and therefore should be used only if a sufficiently large number of training samples are available

7.2 Training Of Adaptive Neuro-Fuzzy Inference System

The training of an ANFIS involves estimating the values of the premise and the consequent parameters, which map input training samples to their targets with a minimum total sum of squared error. However, the total sum of squared error may decrease indefinitely as a result of the onset of a specialized training on noisy training samples with increasing number of training epochs. The specialized training generates a fuzzy inference system that is over learnt on training samples and therefore has poor generalization capabilities. In order to avoid specialized training, an early stopping procedure (Wang et al., 1994) is used, which involves monitoring the total sum of squared error for an independent set of validation samples at the end

of each training epoch and halting the training when it converges to a minimum.

The attribute table of the combined map gives separate values for source, pathways and trap. For each of this criterion, the values are divided into training data and validation data in the ratio of 70:30 respectively. Each of the training data is trained separately in ANFIS and validated. Finally, the classification dataset is fed into the ANFIS model and the output is obtained. The number of epochs set for training the classification dataset is determined from the training and validation dataset. The point where the validation data goes to the minimum and then raises up is taken as the best epoch to train the classification data. The procedure followed is depicted below in the figures 28 to 36.

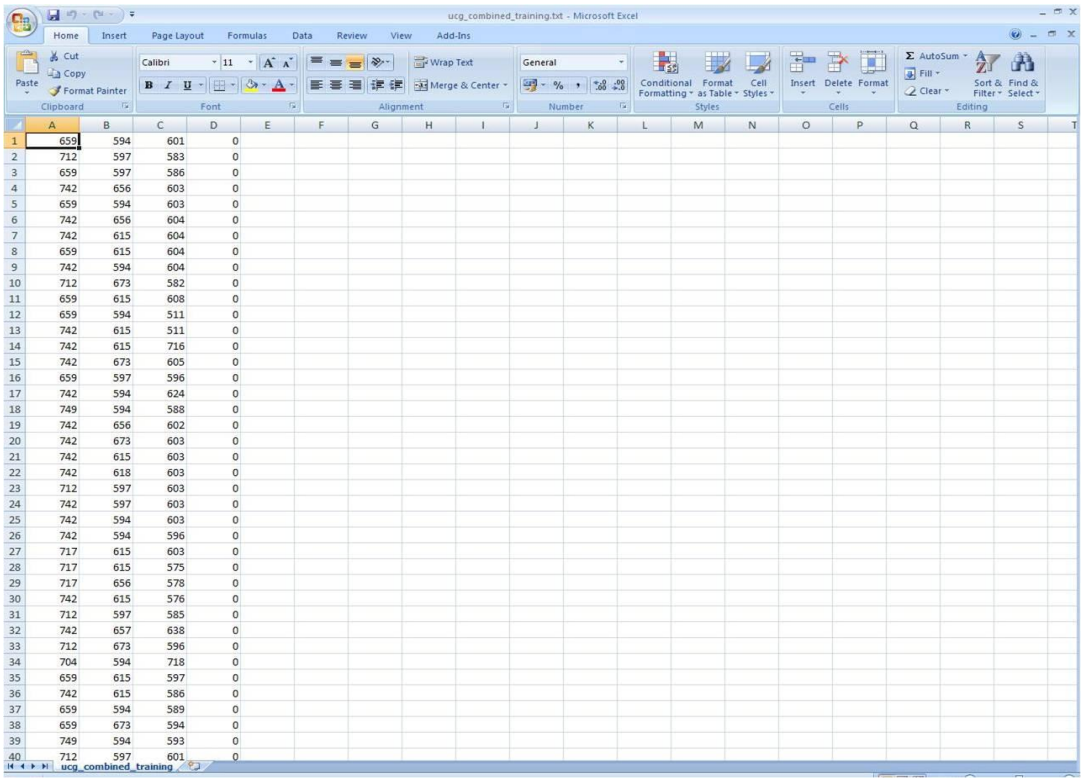

	A	B	C	D
1	659	594	601	0
2	712	597	583	0
3	659	597	586	0
4	742	656	603	0
5	659	594	603	0
6	742	656	604	0
7	742	615	604	0
8	659	615	604	0
9	742	594	604	0
10	712	673	582	0
11	659	615	608	0
12	659	594	511	0
13	742	615	511	0
14	742	615	716	0
15	742	673	605	0
16	659	597	596	0
17	742	594	624	0
18	749	594	588	0
19	742	656	602	0
20	742	673	603	0
21	742	615	603	0
22	742	618	603	0
23	712	597	603	0
24	742	597	603	0
25	742	594	603	0
26	742	594	596	0
27	717	615	603	0
28	717	615	575	0
29	717	656	578	0
30	742	615	576	0
31	712	597	585	0
32	742	657	638	0
33	712	673	596	0
34	704	594	718	0
35	659	615	597	0
36	742	615	586	0
37	659	594	589	0
38	659	673	594	0
39	749	594	593	0
40	712	597	601	0

Fig 28 Training points of the classification dataset

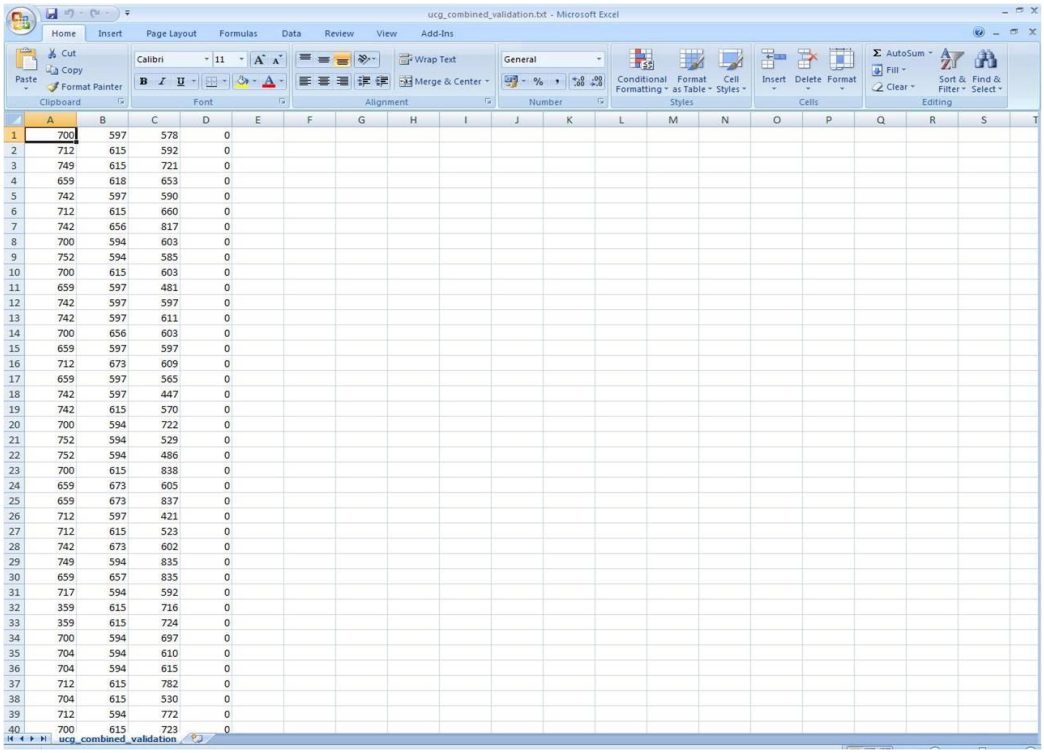

	A	B	C	D
1	700	597	578	0
2	712	615	592	0
3	749	615	721	0
4	659	618	653	0
5	742	597	590	0
6	712	615	660	0
7	742	656	817	0
8	700	594	603	0
9	752	594	585	0
10	700	615	603	0
11	659	597	481	0
12	742	597	597	0
13	742	597	611	0
14	700	656	603	0
15	659	597	597	0
16	712	673	609	0
17	659	597	565	0
18	742	597	447	0
19	742	615	570	0
20	700	594	722	0
21	752	594	529	0
22	752	594	486	0
23	700	615	838	0
24	659	673	605	0
25	659	673	837	0
26	712	597	421	0
27	712	615	523	0
28	742	673	602	0
29	749	594	835	0
30	659	657	835	0
31	717	594	592	0
32	359	615	716	0
33	359	615	724	0
34	700	594	697	0
35	704	594	610	0
36	704	594	615	0
37	712	615	782	0
38	704	615	530	0
39	712	594	772	0
40	700	615	723	0

Fig 29 Validation points of the classification dataset

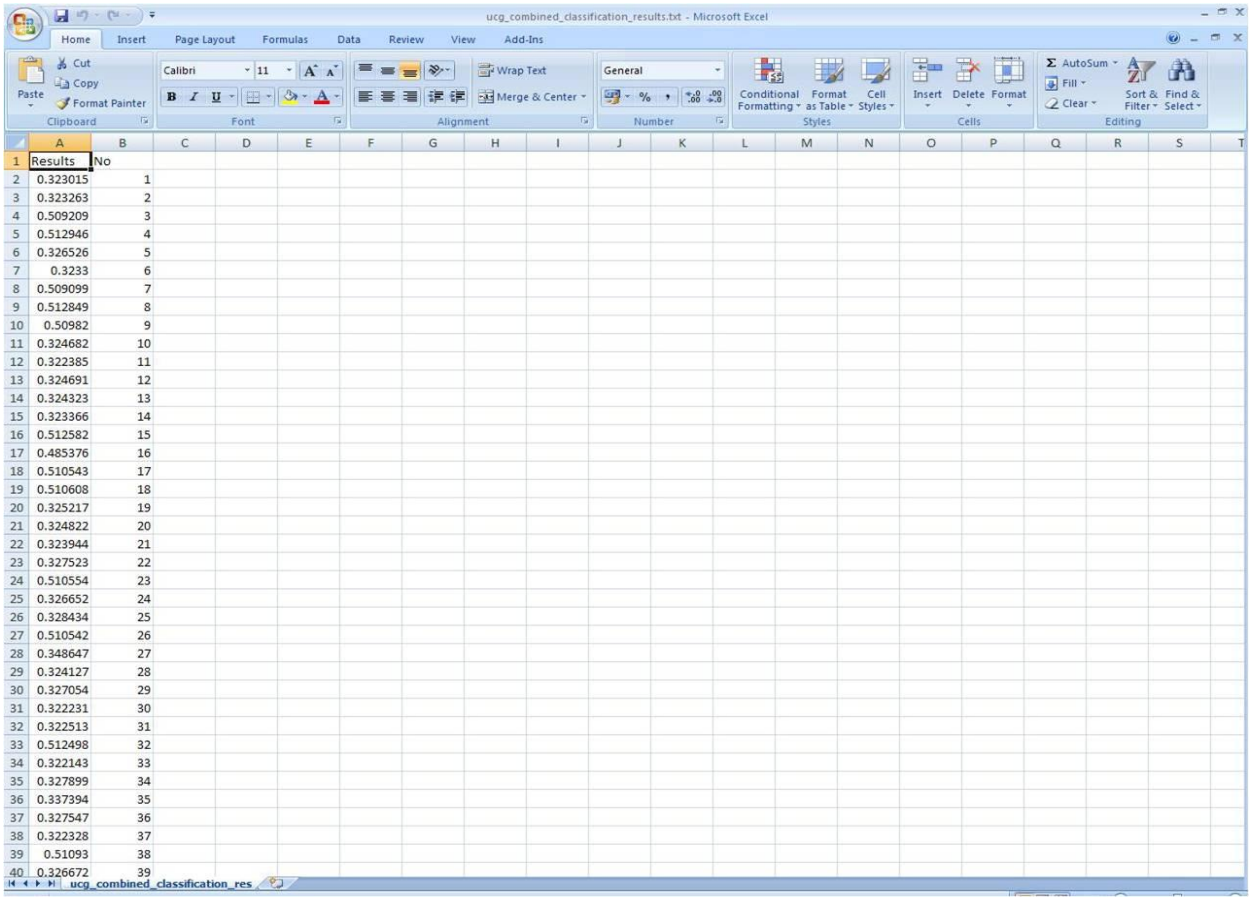

	A	B
1	Results	No
2	0.323015	1
3	0.323263	2
4	0.509209	3
5	0.512946	4
6	0.326526	5
7	0.3233	6
8	0.509099	7
9	0.512849	8
10	0.50982	9
11	0.324682	10
12	0.322385	11
13	0.324691	12
14	0.324323	13
15	0.323366	14
16	0.512582	15
17	0.485376	16
18	0.510543	17
19	0.510608	18
20	0.325217	19
21	0.324822	20
22	0.323944	21
23	0.327523	22
24	0.510554	23
25	0.326652	24
26	0.328434	25
27	0.510542	26
28	0.348647	27
29	0.324127	28
30	0.327054	29
31	0.322231	30
32	0.322513	31
33	0.512498	32
34	0.322143	33
35	0.327899	34
36	0.337394	35
37	0.327547	36
38	0.322328	37
39	0.51093	38
40	0.326672	39

Fig 30 Classification results obtained from ANFIS model

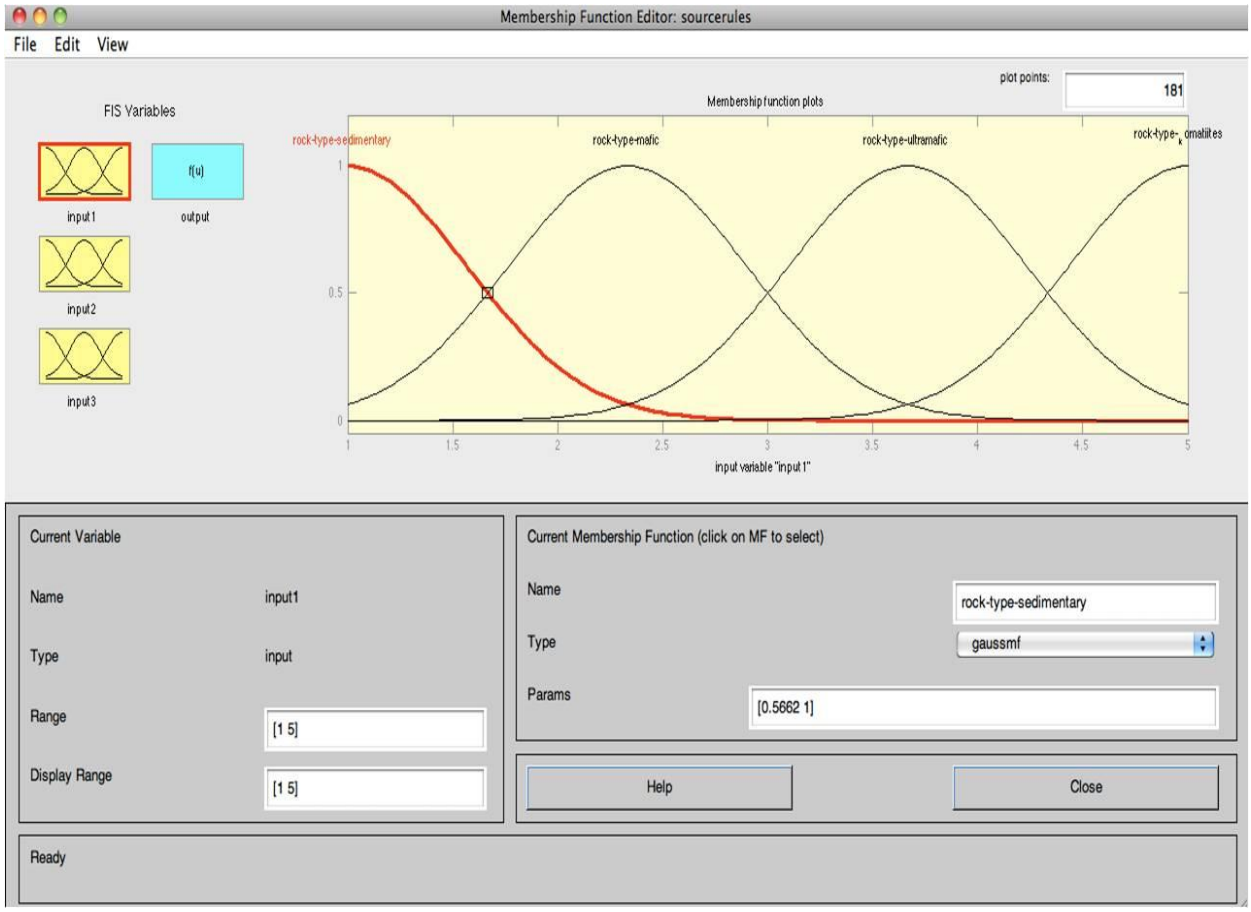

Fig 31 ANFIS GUI showing the membership function of the source criterion

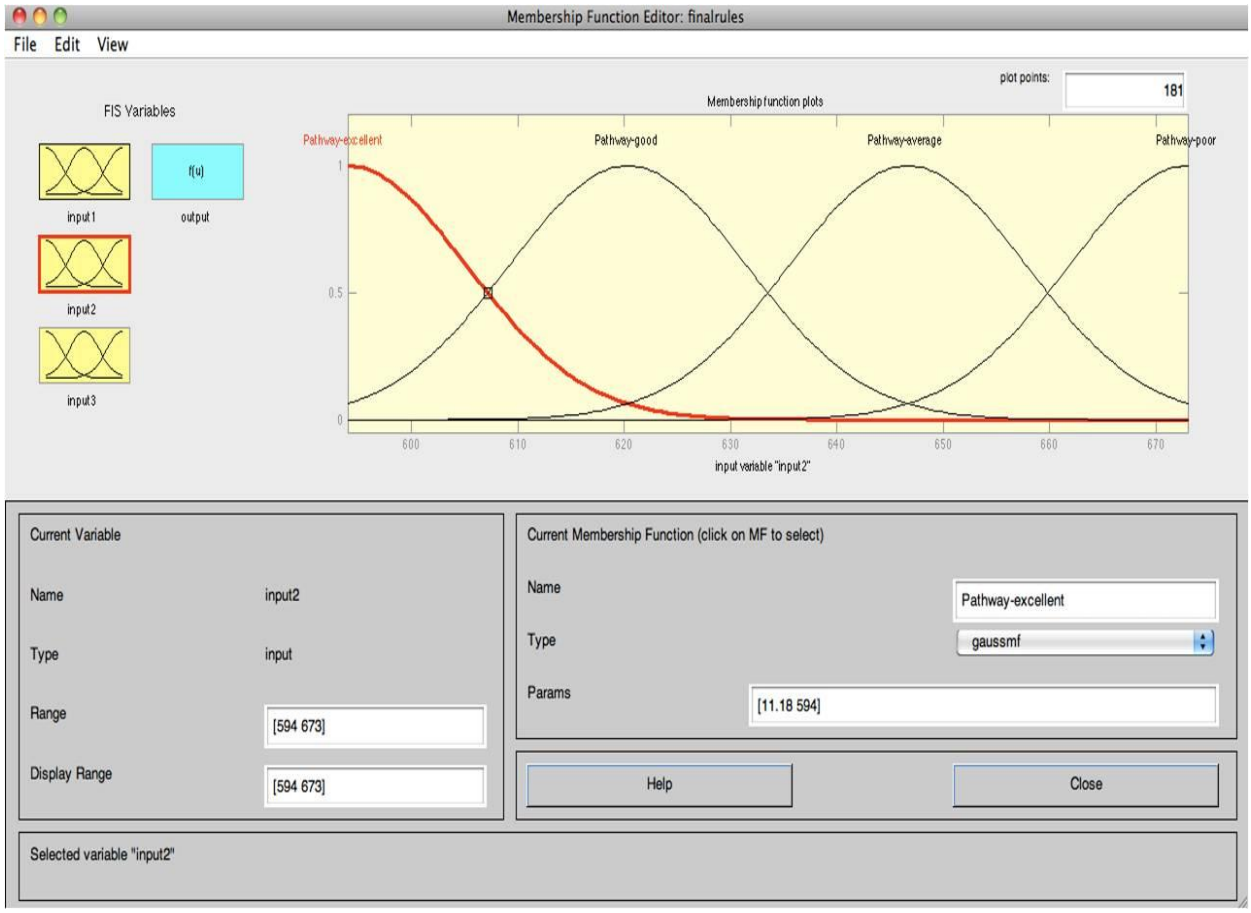

Fig 32 ANFIS GUI representing the membership function of the pathway criterion

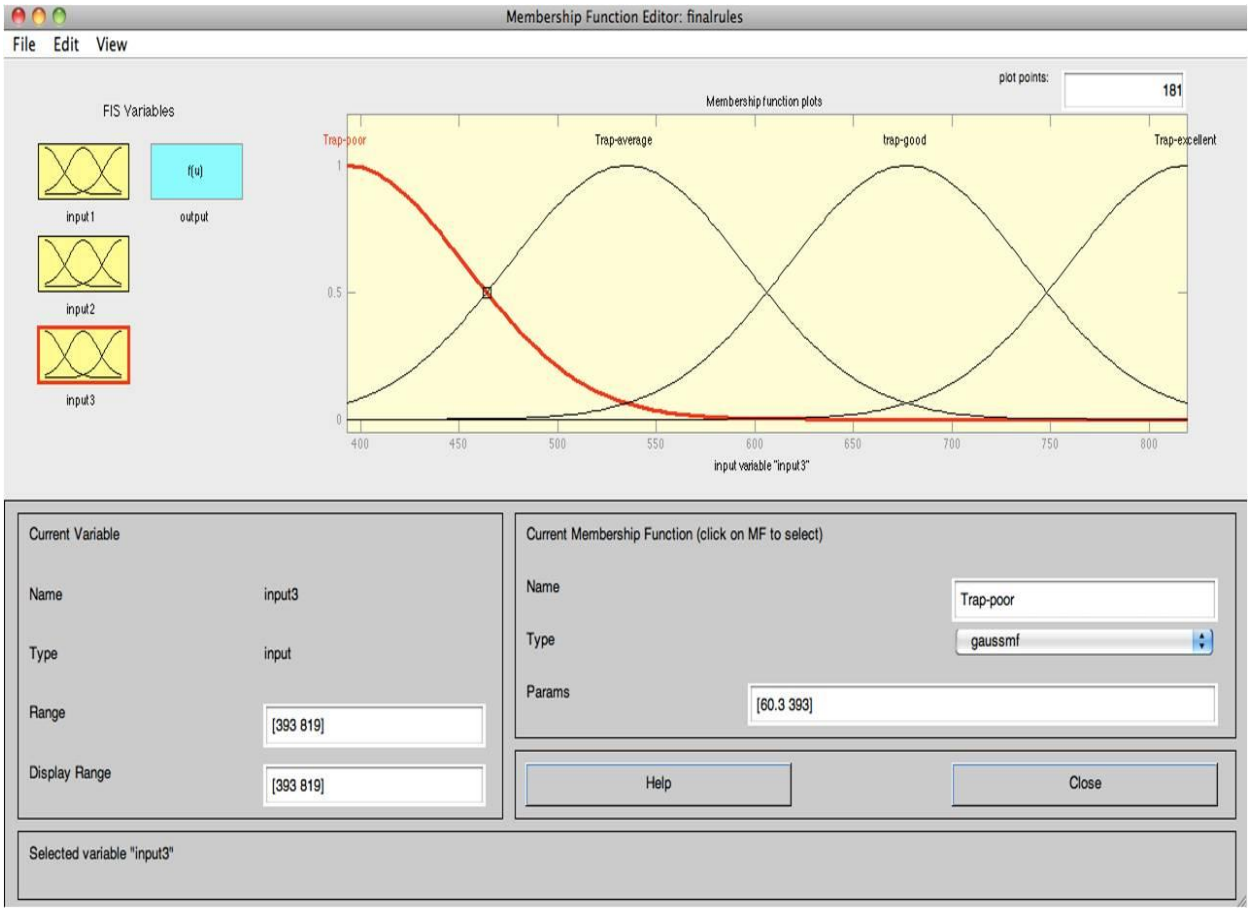

Fig 33 ANFIS GUI showing the membership function of the saturation criterion

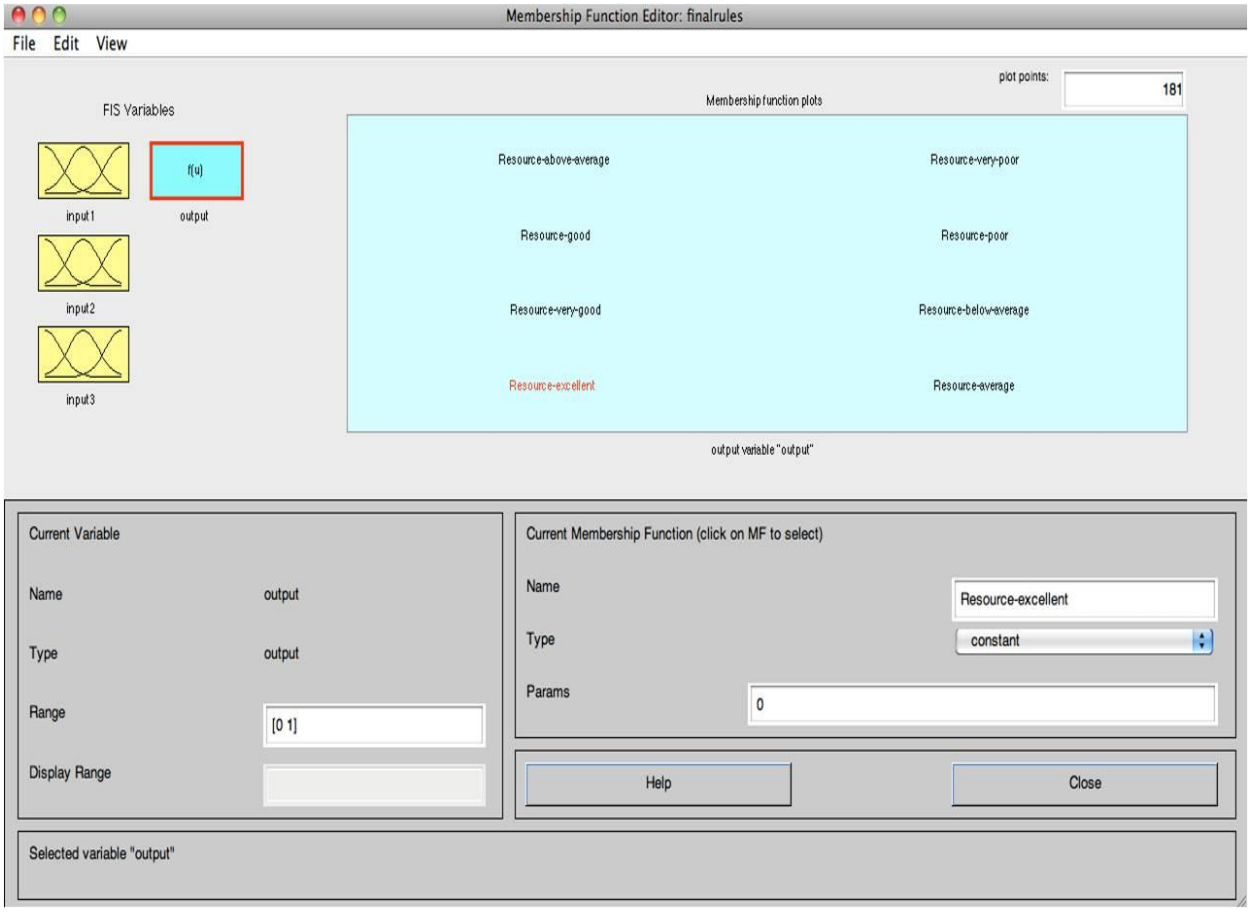

Fig 34 ANFIS GUI showing the Fuzzy rules

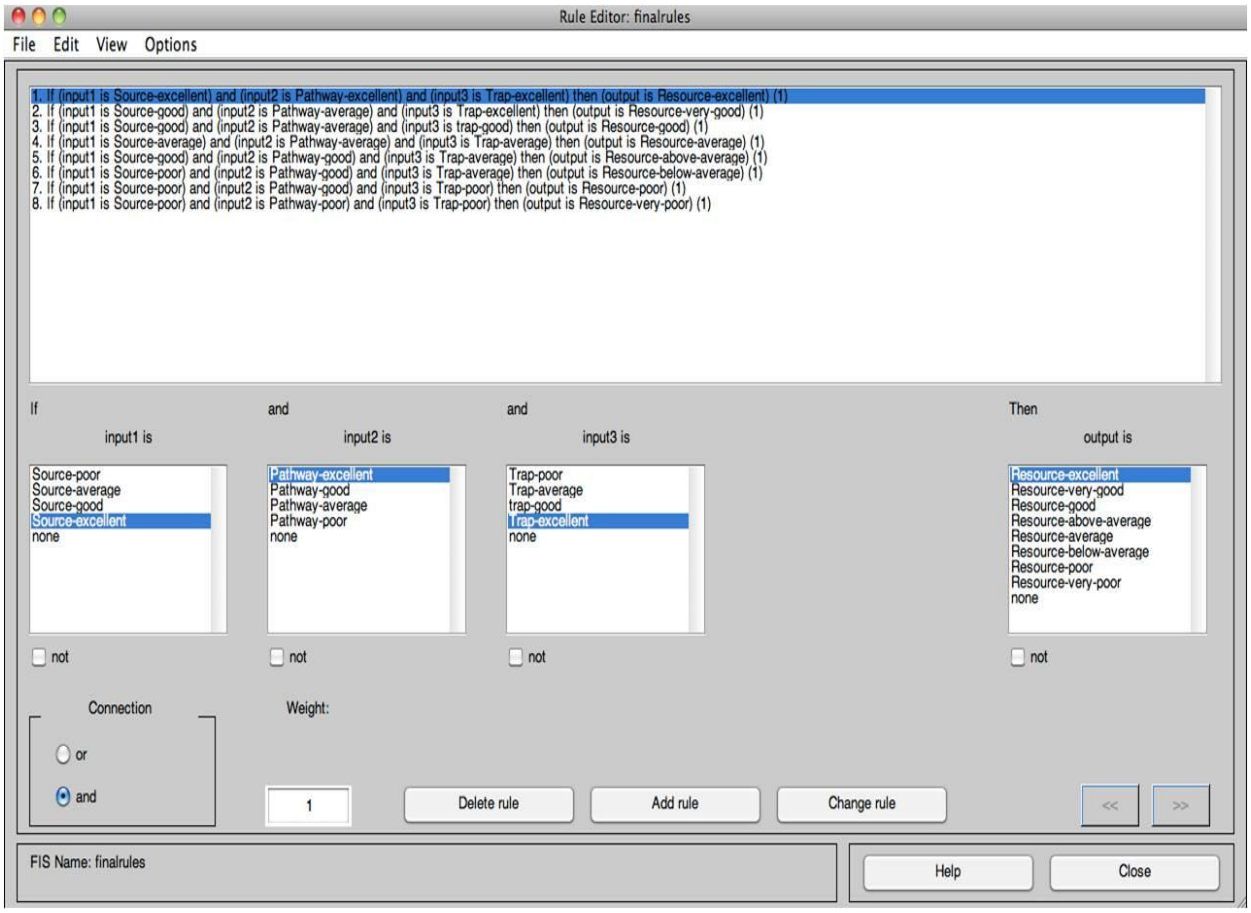

Fig 35 the eight fuzzy rules adopted for the classification output

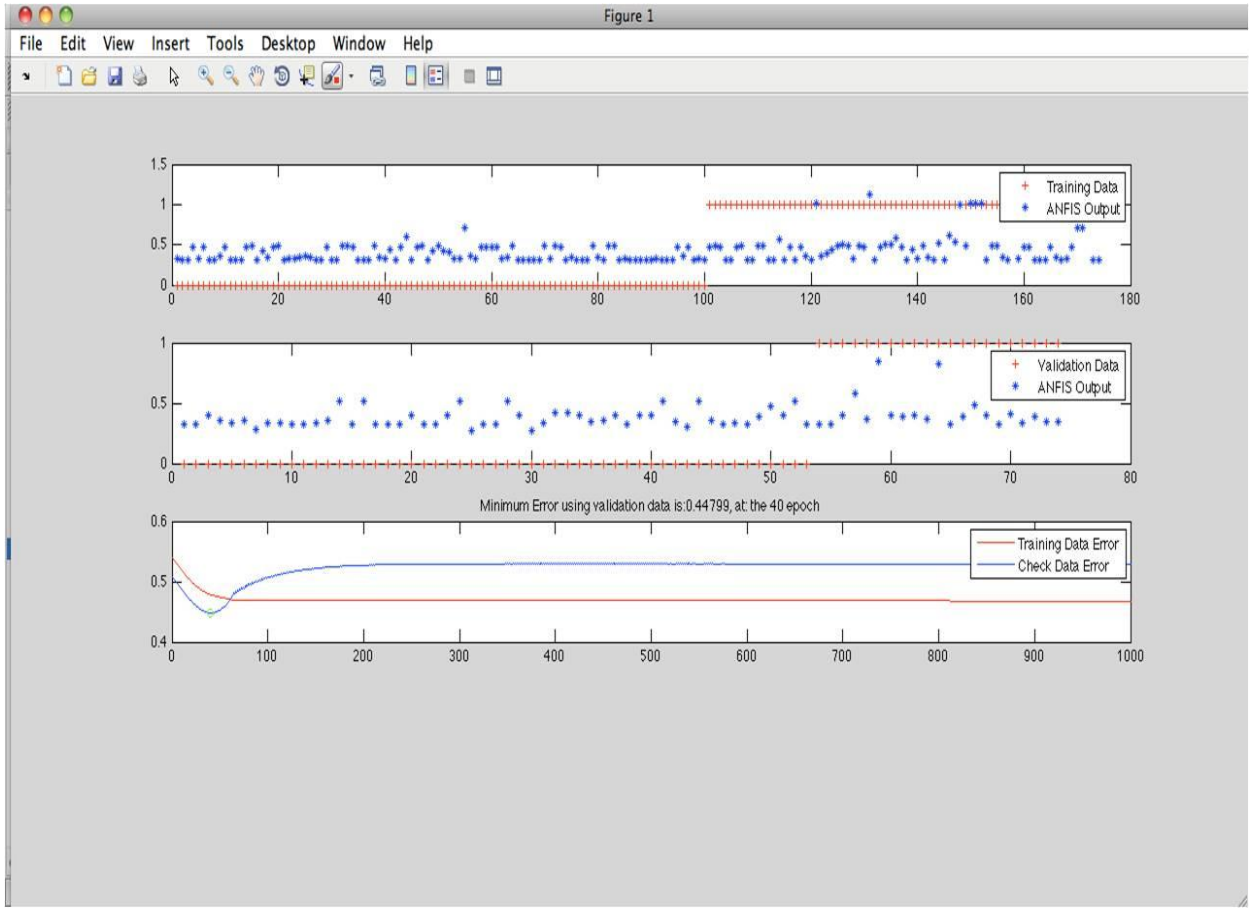

Fig 36 ANFIS GUI depicting the number of epochs to be adopted to train the classification dataset

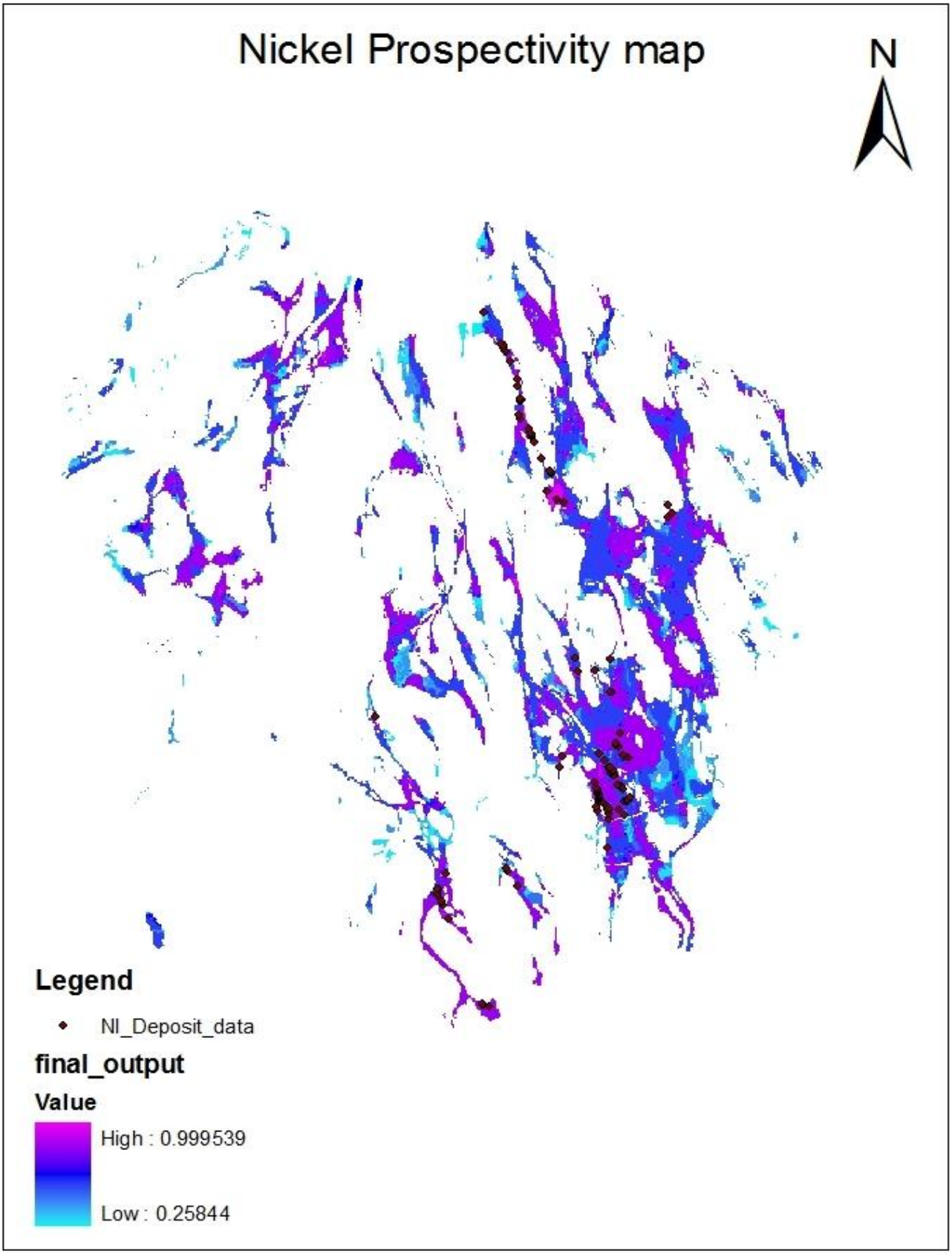

Fig 37 Magmatic Nickel Sulphide Prospectivity map using ANFIS

The above figure shows the probability of presence of the magmatic nickel sulphide in the greenstone belt region and it can be seen that there is 99% possibility for the presence of the mineral. The already known Nickel deposit data points are added to the map to check the accuracy and effectiveness of the results. It can be well seen that the high prospectivity areas lie around the known nickel deposit data, thus confirming the efficiency of ANFIS in mineral prospectivity mapping.

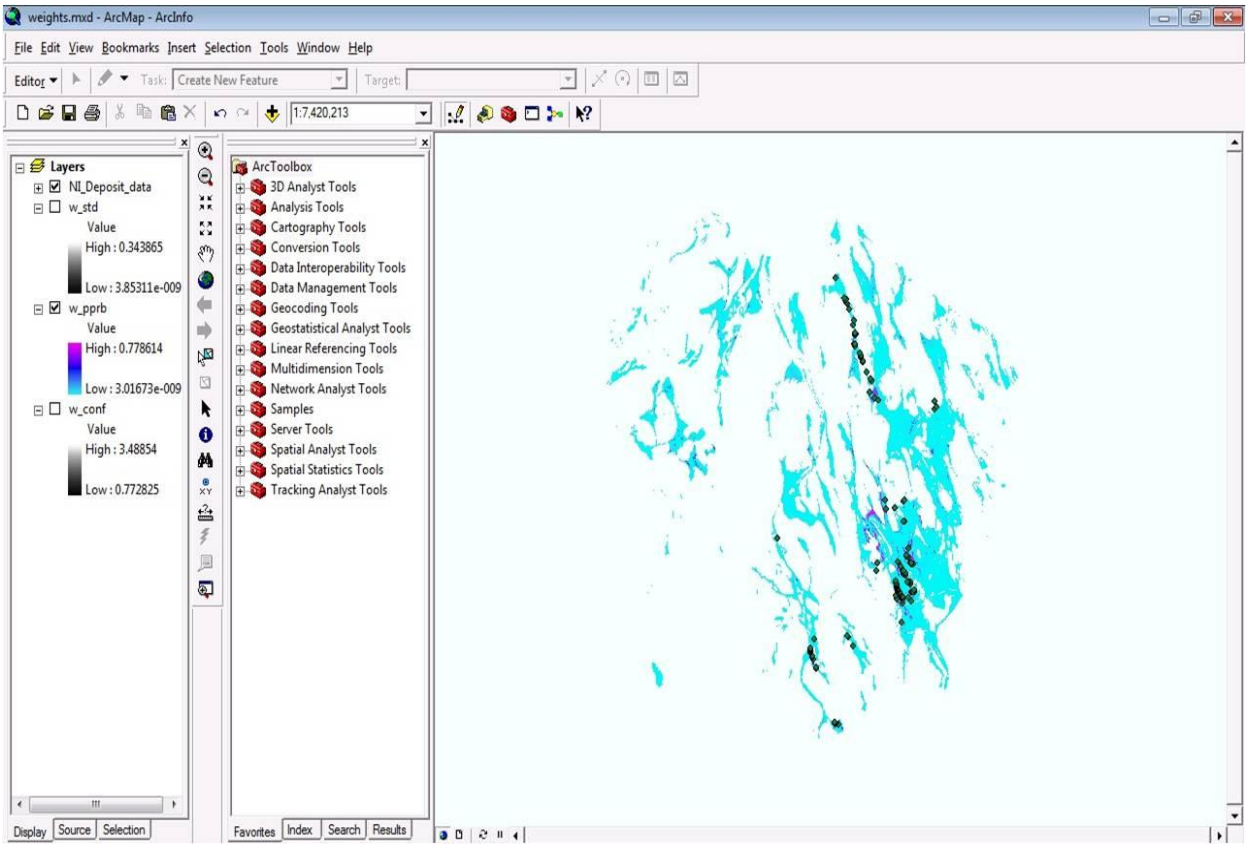

Fig 38 Magmatic Nickel Sulfide Prospectivity Map of the Greenstone Belts region using Weights of Evidence method

By comparing the results obtained by using ANFIS and Weights of Evidence, it can be seen that the ANFIS model predicted 99% of the study region as prospectivity zone whereas only 77% of the study area is delineated as prospectivity zone by the weights of evidence. This highlights the efficiency and accuracy of the ANFIS model over the traditional Weights of Evidence in mineral prospectivity mapping.

8. CONCLUSION

The application of ANFIS predicted about 70% of the validation deposits in prospective zones that occupy about 9% of the total area occupied by the greenstone belts in the Craton. The area within the proximity of one unit cell from the high prospectivity zones can be considered prospective because the boundaries of polygonal features become jagged when converted to raster format and as a result, some area that is originally within a polygon falls outside the rasterized polygon. This preliminary study also shows that by implementing a fuzzy inference system in the framework of an adaptive neural network, the hybrid neuro-fuzzy approach provides a robust data-based method for estimating the parameters of the fuzzy inference system. While the weights of evidence predict only 77% of the study area as most prospective for magmatic nickel sulfide, ANFIS estimates 99.5% of the region as the prospective zones.

9. DISCUSSION

9.1. Favourable rock type for mineralization

The prospective areas in this study are generally confined to the komatiite and ultramafic rocks of the Craton. Although the presence of komatiite is considered a key exploration criterion for magmatic nickel sulfide deposits in the Yilgarn, about 38% of the komatiites are mapped as unprospective by the models. The implication is that komatiites cannot be used in isolation to select exploration targets. This is consistent with the mineral systems approach, which considers mineral deposits as focal points of much larger mass flux and energy systems and requires that several critical components, in particular, source, transport pathways and trap environments must be present in order to form mineral deposits (Wyborn et al., 1994). The mineral systems approach explicitly precludes the formation of mineral deposits where one or more essential components are missing. Accordingly, although komatiites in the Yilgarn craton are important source and carrier rocks of nickel, magmatic nickel sulfide deposits form only where other critical components in particular sulfur saturation, also occur.

9.2 Importance of Sulphur Saturation

However, it must be pointed out that sulfur saturation is best predicted using detailed volcanologic and geochemical criteria on the deposit scale. At the

scale of the present analysis (1:500,000, which was the scale of the geological map used as one of the primary data sources), it was not possible to procure adequate public-domain datasets for generating spatial proxies for all processes that could lead to sulfur saturation of nickel-rich source magma and precipitation of nickel sulfides. The predictor maps derived using the regional-scale geochemical datasets in the present study can therefore be considered only as indicative of sulfur saturation, although they show reasonably good spatial associations with known mineral deposits. The ANFIS model performs better than the Weights of Evidence model in predicting the known mineral deposits in the Craton. Thus, GIS-based modeling techniques provide a fast and economic way to delineate prospective target areas on regional-scale, based on public-domain exploration datasets.

Appendix A

MATLAB Codes Used

```
threshold = 0.5

b = uint8(Res_trnData_prediction>=threshold);

b_trnData = uint8(trnData(:,n));

[C,order] = confusionmat(b_trnData,b);

trnData_overall_accuracy = (C(1,1)+C(2,2))/sum(sum(C));

b = uint8(Res_chkData_prediction>=threshold);

b_chkData = uint8(chkData(:,n));

[C,order] = confusionmat(b_chkData,b);

chkData_overall_accuracy = (C(1,1)+C(2,2))/sum(sum(C));

% Load the training, validation, and fuzzy-rules files

% trnData = load('sulfur saturation.txt');

% chkData = load('Validation_S_Saturation.txt');

% in_fis = readfis('saturationrules');

trnData = load('trnData.txt');

chkData = load('validation-source-final.txt');

ClassData = load('source-class_Le.txt');

in_fis = readfis('initfis');

%% ANFIS
```

% set training epoch number

epochnum=1000;

% trnOpt: a vector of training options. When a training option is entered as NaN, the default options is in force. These options are as follows:

% trnOpt(1): training epoch number (default: 10)

% trnOpt(2): training error goal (default: 0)

% trnOpt(3): initial step size (default: 0.01)

% trnOpt(4): step size decrease rate (default: 0.9)

% trnOpt(5): step size increase rate (default: 1.1)

trnOpt=[epochnum,0.25,0.01,0.9,1.1];

% dispOpt: a vector of display options that specify what message to display in the MATLAB Command Window during training. The default value for a display option is 1, which means that the corresponding information is displayed. A 0 means the corresponding information is not displayed. When a display option is entered as NaN, the default options will be in force. These options are as follows:

% dispOpt(1): ANFIS information, such as numbers of input and output membership functions, and so on (default: 1)

% dispOpt(2): error (default: 1)

% dispOpt(3): step size at each parameter update (default: 1)

% dispOpt(4): final results (default: 1)

```
dispOpt=[1,1,0,1];
% Training routine for Sugeno-type Fuzzy Inference System
% pls refer to matlab help document
% the last input parameter for anfis indicate the optimization method used in membership function parameter training:
% 1 = hybrid method; 0 = backpropagation method. The default method is the hybrid method, which is a combination of least-squares estimation with backpropagation. The default method is invoked whenever the entry for this argument is anything but 0.
[out_fis,error,stepsize,chkFis,chkErr] = anfis(trnData,in_fis,trnOpt,dispOpt,chkData,0);
%% Output - Display the results
% shows the differences between original label (in training dataset) and ANFIS output
[m,n]=size(trnData);
X_axis_train=[1:m];
subplot(4,1,1)
plot(X_axis_train',trnData(:,n),'r+',X_axis_train',evalfis(trnData(:,1:(n-1)),out_fis),'b*');
legend('Training Data','ANFIS Output');
```

```
% shows the differences between original label (in validation dataset) and ANFIS
output
[m,n]=size(chkData);
X_axis_check=[1:m];
subplot(4,1,2)
plot(X_axis_check',chkData(:,n),'r+',X_axis_check',evalfis(chkData(:,1:(n-
1)),chkFis),'b*');
legend('Validation Data','ANFIS Output');
% shows the error trends of training dataset and validation dataset
X_axis_epoch=[1:epochnum];
subplot(4,1,3)
plot(X_axis_epoch',error,'r',X_axis_epoch',chkErr,'b');
legend('Training Data Error','Check Data Error');
% indicate the best stop epoch
chkErr_min=min(chkErr);
chkErr_min_location=find(chkErr==chkErr_min);
hold on
plot(chkErr_min_location,chkErr_min,'go');
hold off
```

string=['Minimum Error using validation data is:', num2str(chkErr_min), ', at: the ',num2str(chkErr_min_location), ' epoch'];

title(string)

%% Export results

Res_trnData_prediction=evalfis(trnData(:,1:(n-1)),out_fis); % anfis prediction results of training data

Res_trnData_error=error; % errors of training data

Res_chkData_prediction=evalfis(chkData(:,1:(n-1)),chkFis); % anfis prediction results of validation data

Res_chkData_error=chkErr; % errors of validation data

%% Classification

[cm,cn]=size(ClassData);

class_default=ones(1,cm,1)';

clsData=[ClassData,class_default];

% keep all the parameters here the same to line 60

[out_fis,error,stepsize,clsFis,clsErr] = anfis(trnData,in_fis,trnOpt,dispOpt,clsData,0);

% shows the differences between original label (in classification dataset) and ANFIS output

X_axis_check=[1:cm];

subplot(4,1,4)

plot(X_axis_check',clsData(:,(cn+1)),'r+',X_axis_check',evalfis(clsData(:,1:cn),cls Fis),'b');*

legend('Classification Data','ANFIS Output');

Res_clsData_prediction=evalfis(clsData(:,1:(n-1)),clsFis); % anfis prediction results of validation data

Res_clsData_error=clsErr; % errors of validation data

Appendix B

Google Earth Maps

The Yilgarn Craton boundary and the greenstone belts boundary are laid to Google Earth for better visualization purposes. The final prospectivity map obtained is also overlaid onto the Google map and they are shown in the following figures from figure 39 and 41.

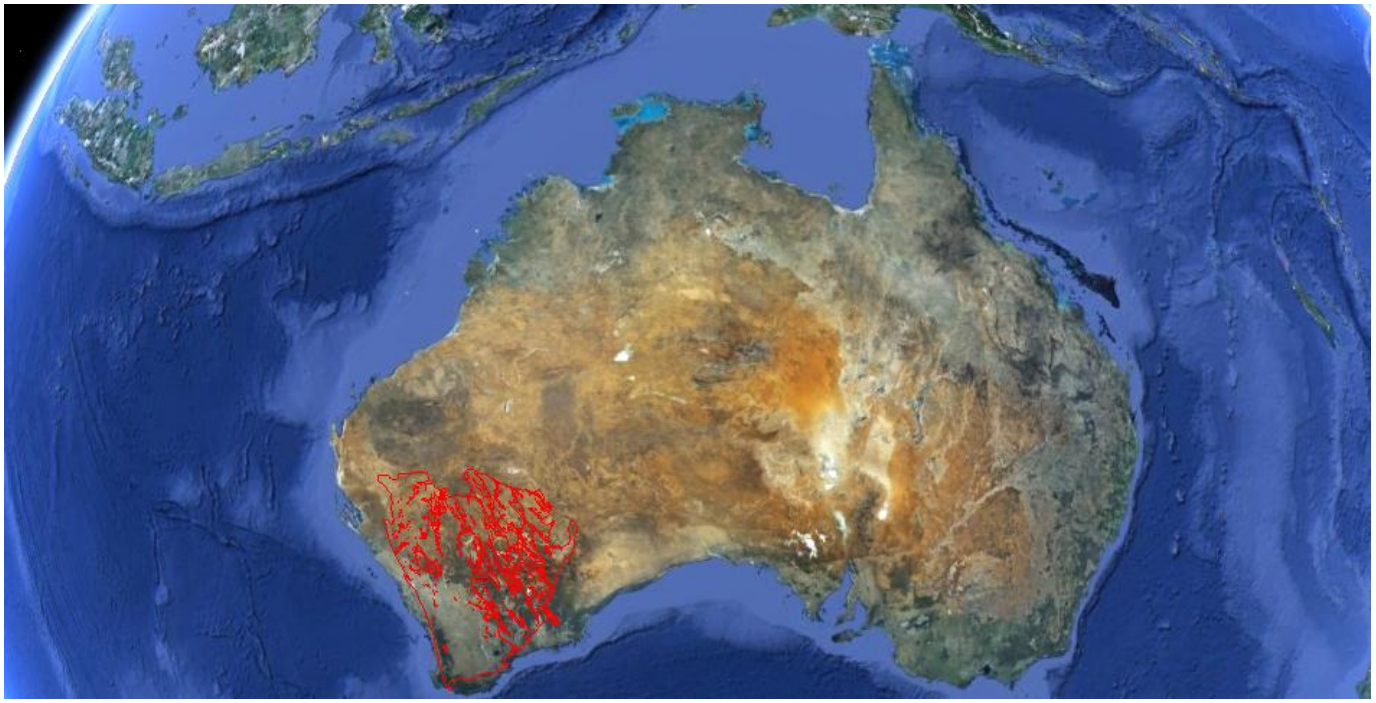

Fig 39. Google Earth window showing the location of the study area in the western region of Australia.

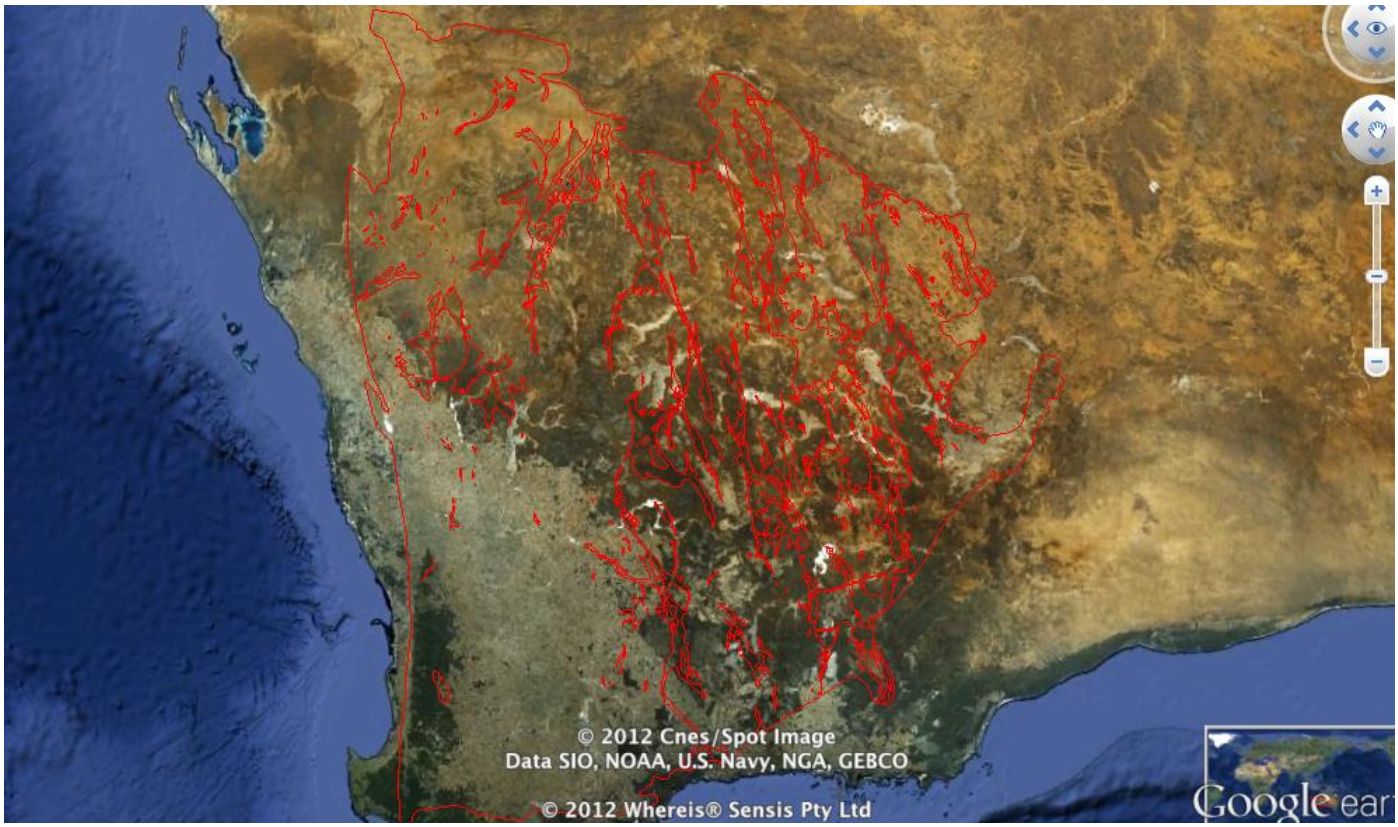

Fig 40 Google Earth window showing the boundaries of the Yilgarn Craton and the Greenstonebelts

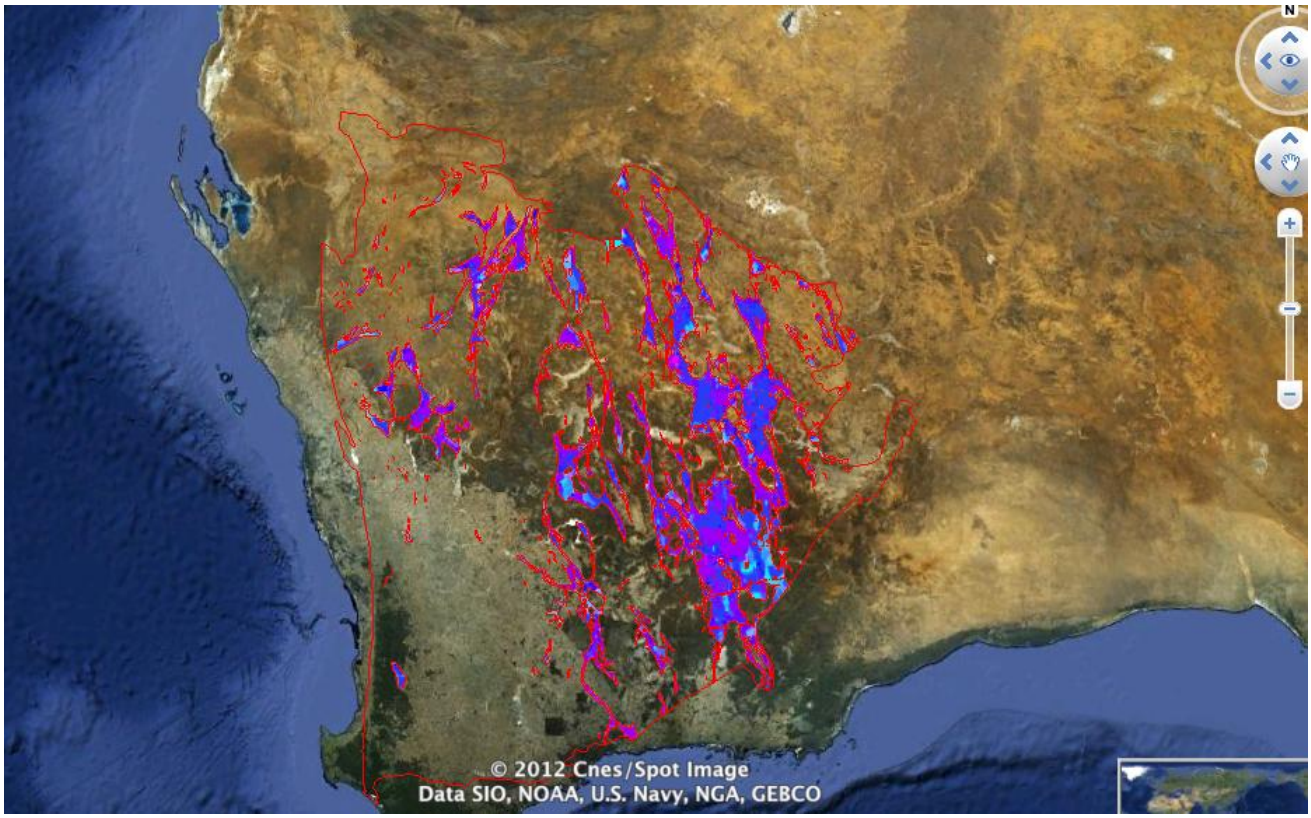

Fig 41 Magmatic Nickel Sulphide Prospectivity map obtained by ANFIS model imposed between the boundaries of Greenstone belt and Yilgarn Craton

References

Abeysinghe, P.B., Flint, D.J., 2007. Nickel and cobalt in Western Australia: commodity review for 2005. Department of Industry and Resources, WA, Record, 12.46 p.

Adriano Cruz, ANFIS: Adaptive Neuro-Fuzzy Inference Systems, Mestrado NCE, IM, UFRJ

Alok Kumar Porwal , 2006, Mineral Potential Mapping with Mathematical Geological Models, International Institute for Geo-information Science and Earth Observation, Enschede, The Netherlands, ITC dissertation number 130

A.Porwal, I. Gonzalez-Alvarez, V.Markwitz, T.C.McCuaig, A.Mamuse, 2010, Weights-of-evidence and logistic regression modeling of magmatic nickel sulfide prospectivity in the yilgarn Craton, Western Australia, Ore Geology Reviews, 38, 184-196.

Azar and Ahmad Taher, Adaptive Neuro-Fuzzy Systems, Electrical Communications and Electronics Systems Engineering department, Modern Science and Arts University (MSA), Egypt.

Barnes, J.S., Hill, R.E.T., Perring, C.S., Dowling, S.E., 2004. Lithogeochemical exploration for komatiite-associated Ni-sulfide deposits: strategies and limitations. Mineralog and Petrol. 82,259-293.

Brand, N.W., 1999. Element ratios in nickel sulfide exploration: vectoring towards ore environments. J. of Geochem.Exploration 67, 145-165.

Good, I.J., Bernardo J.M., DeGroot M.H., Lindley D.V., Smith A.F.M., 1985, Weight of Survey: A Brief survey. Virginia Polytechnic Institute and State University

Hoang Bac Bui, QuocPhi Nguyen, VanTrung Nguyen, GIS-Based Weights-of-EVIDENCE Modeling for landslide susceptibility mapping at Jaechon area, Korea, Department of Earth System Sciences, Yonsei University, Seoul, Korea, Department of Geotechnical and Environmental Engineering, Paichai University, Korea.

Hoatson, D.H., Jaireth, S., Jacques, L., 2006. Magmatic nickel sulfide deposits in Australia: characteristics, resources and potential. Ore Geol.Rev.29, 177-241.

Hongmei Wang, Guoray Cai, Qiuming Cheng, Data Integration Using Weights of Evidence Model: Applications in Mapping Mineral Resource Potentials

Jang, J.S.R., 1993. ANFIS: Adaptive-network-based fuzzy inference system. IEEE Transactions on Systems, Man and Cybernetics, v. 23, p. 665-685.

Jyh-Shing, Roger Jang, 1993, ANFIS: Adaptive-Network-Based Fuzzy Inference System. IEEE Transactions on Systems, man and cybernetics, vol.23, No.3

Keays, R.R., 1995. The role of komatiite and picritic magmatism and S-saturation in the formation of ore deposits. Lithos 34, 1-18.

Lesher, C.m., Burnham, O.M., keays, R.R., Barnes, S.J., Hulbert, L., 2001. Geochemical discrimination of barren and mineralized komatiites associated with magmatic Ni-Cu-(PGE) sulfide deposits. Can. Mineralog. 39, 673-696.

Lightfoot, P.C., 2007. Advances in Ni-Cu-PGE sulfide deposits models and implications for exploration technologies. Ore deposits and exploration technology. In: Milkereit, B. (Ed.), Proceedings of Exploration 07: Fifth Decennial International Conference on Mineral Exploration, pp.629-646.

Mamdani, E.H., 1974. Applications of fuzzy algorithm for control of a simple dynamic plant. Proceedings of IEEE, v. 121(12), p. 1585-1588.

Mamdani E.H., and Assilian S., 1975. An Experiment in Linguistic Synthesis with a Fuzzy Logic Controller. International Journal of Man-Machine Studies, v. 7(1), p. 1-13.

Mordjaoui.M and Boudjema, 2001, Forecasting and Modelling Electricity Demand Using Anfis Predictor, Journal of Mathematics and Statistics

Naldrett, A.J., 1997. Key factors in the genesis of Noril'sk. Sudbury, jinchuan, Voisey's Bay and other world-class Ni-Cu-PGE deposits: Implications for exploration. Aust.J. of Earth Sci. 44, 283-315.

Piero P. Bonissone, 2002, Adaptive Neural Fuzzy Inference Systems (ANFIS): Analysis and Applications

Porwal, A., Carranza, E.J.M., and Hale, M., 2003a. Knowledgedriven and data-driven fuzzy models for predictive mineral potential mapping. Natural Resources Research, v. 12(1), p. 1-25.

Sugeno, M., and Kang, G.T., 1988. Structure identification of fuzzy model. Fuzzy Sets and Systems, v. 28, p. 12-33

Sugeno, M., and Tanaka, K., 1991. Successive identification of a fuzzy model and its application to prediction of complex systems. Fuzzy Sets and Systems, v. 42, p. 315-334.

Takagi, T., and Sugeno, M., 1985. Fuzzy identification of systems and its applications to modelling and control: IEEE Transactions on Systems, Man and Cybernetics, v. 15(1), p. 116-132.

Tsukamoto, Y., 1979, An approach to fuzzy reasoning method. In: Gupta, M.M., Ragade, R.K. and Yager, R.R., (Eds.), Advances in Fuzzy Set Theory and Applications, North-Holland, Amsterdam, p. 137-149.

Wang, C., Venkatesh, S.S., and Judd, J.S., 1994, Optimal stopping and effective machine complexity in learning. In Cowan, J.D., Tesauro, G., and Alspector, J., (Eds.), Advances in Neural Information Processing Systems: Morgan Kaufmann, San Francisco, p. 303-310.

Zadeh, L.A., 1973. Outline of a new approach to the analysis of complex systems and decision process. IEEE Transactions on Systems, Man and Cybernetics, v. 3, p. 28-44.